國 立 交 通 大 學

電 子 物 理 研 究 所

碩 士 論 文

在 Dresselhaus-type 介觀量子環中的持續性電流和
自旋密度

PERSISTENT CURRENT AND SPIN DENSITY
IN A MESOSCOPIC DRESSELHAUS-TYPE
QUANTUM RING

研 究 生：吳智偉

指導教授：朱仲夏教授

在 Dresselhaus-type 介觀量子環中的持續性電流和自旋密度

PERSISTENT CURRENT AND SPIN DENSITY IN A MESOSCOPIC DRESSELHAUS-TYPE QUANTUM RING

研 究 生：吳智偉　　　　　　Student：Chih-Wei Wu

指導教授：朱仲夏教授　　　　Advisor：Prof. Chon Saar Chu

國 立 交 通 大 學

電 子 物 理 研 究 所

碩 士 論 文

A Thesis
Submitted to Department of Electrophysics
College of Science
National Chiao Tung University
in Partial Fulfillment of the Requirements
for the Degree of
Master
in
Electrophysics

July 2009
Hsinchu, Taiwan, Republic of China

中華民國九十八年七月

在 Dresselhaus-type 介觀量子環中的持續性電流和自旋密度

研究生：吳智偉　　　　　　　　　　指導教授：朱仲夏教授

國立交通大學

電子物理研究所

摘要

　　本論文的工作主要是去探究以及了解在有限寬的介觀環裡 Dresselhaus 自旋軌道交互作用效應的物理意涵，包含有和沒有外加磁通量兩種情況。而自旋密度和持續性電流是我們關注的物理量。特別地，我們藉由個別獨立打開 Dresselhaus 自旋軌道交互作用和磁通量，去仔細分析本徵態和能譜來得到物理意涵。

　　在打開 Dresselhaus 自旋軌道交互作用強度的情況下，我們證明所有的能階都是 Kramer's type 的雙重簡併，以及藉由能階排斥原理和相對基底本徵態比重來瞭解能譜的趨勢。在弱自旋軌道交互作用場的範疇下，能譜和 Dresselhaus 自旋軌道交互作用強度成二次方關係，此結果與我們的微擾分析相同。

　　在漸增磁通量的情況下，我們呈現了 Kramer 簡併態的分裂，以及確認分裂後能譜的物理原因。對於在打開 Dresselhaus 自旋軌道交互作用或磁通量後的本徵態，我們發展了一套有系統的方法去得到它的通式。我們也計算了一個本徵態所對應的自旋密度和淨 z 方向投影自旋量。當系統中有 N 個電子時，總合每個本徵態就能得到全部的總量。

Persistent current and spin density in a mesoscopic Dresselhaus-type quantum ring

Student: Chih-Wei Wu   Advisor: Chon-Saar Chu

Department of Electrophysics

National Chiao-Tung University

Abstract

The work of this thesis is to explore and to understand physical insights on the effects of Dresselhaus spin-orbit interaction (DSOI) in a finite width mesoscopic ring, both with and without a magnetic flux. The physical quantifies of interest are the spin density and persistent current. Specifically, our insight is obtained from a detail analysis of the eigenstates and the energy spectrum as the DSOI is turned on and, independently, when the magnetic flux is turned on.

For the case of turning on of the DSOI strength, we demonstrate that all energy levels are doubly degenerate, of the Kramer's type, and the trend of the energy spectrum is understood by level repulsions and the relative weighting between the constituent bases state ket. The energy spectrum depends on the DSOI quadratically in the weak SOI field regime, and this is consistent with our perturbation result.
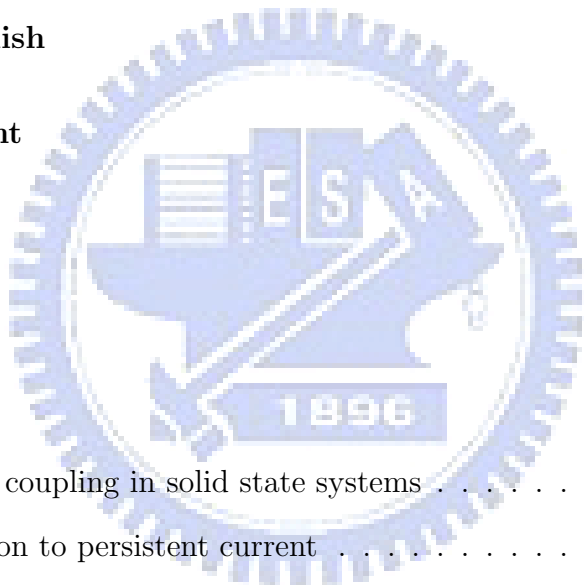
For the case of increasing the magnetic flux, we show that the Kramer degenerate states split and the physical reason for the subsequent order in the energy splitting is identified. For the eigenstate in the presence of the DSOI and the magnetic flux, we have developed a systematic way to produce its general form. We have calculated the spin density and the net spin S_z of an eigenstate. Summing these gives us the total when there are N electrons in the system.

致謝

　　自我實現，一直是我成長的基本動力，我有夢，就會勇敢去追。回想起二年前，在教書之餘，抓緊時間挑燈夜讀，為的不僅只是提升專業知識、攻讀學位，更重要的是自我實現的完成。如今，正值收割豐碩果實的時候，我心存感激，由衷感謝朱老師仲夏的耐心指導，不管是在研究上或做人處事的態度上都讓我獲益良多，而研究室的學長同學們也在各方面給予我莫大的幫助，尤其是律堯和志宣，慶幸有他們的協助，我才能如期完成研究。在交大七百多個日子裡，很感謝研究室的夥伴們陪我一同度過，志雄、律堯、榮興、志宣、吉偉、昆宜、冠誼，重訓室的肌肉男們陪我一起成長，瑞甫、冠旭、家權、阿草、霸子…，第二餐廳裡老陳快餐的歐巴桑偷偷免費幫我加滷蛋，以及我的女友怡佩，一路上的支持與鼓勵，讓我沒有後顧之憂。謝謝你們，謝謝！

Contents

List of Figures

Chapter 1

Introduction

Today, more and more new artificial technology is built upon charge-based electronics where spin of an electron, however, was neglected in the technology application before. This stream of neglecting spin in the application sector may have set a different schedule in the past decades when spintronics were proposed and realized.

In order to control electrons on spin transport and spin accumulation in semiconductors, we should invoke the spin-orbit interaction (SOI). According to the physical origin of the SOI, the SOI can be divided into intrinsic and extrinsic types, the more detail will be discussed in the next section. In other way, the quantum ring is a popular device which can be designed as calculation units, therefore, many scientists get into this area and discover many interesting physical phenomenon.

Although persistent current with Rashba spin-orbit interaction [1] in one-dimensional ring has been discussed generally, few researches focus on Dresselhaus spin-orbit interaction [2] in finite width ring. We propose two important points of view about our motivation. First, one-dimensional ring is an ideal case which can not be performed by experiment exactly, and it is impossible to discuss the spin density in r-direction,too. Therefore, we suggest a finite width ring-shaped potential pattern to study the spin accumulation and the persistent current realistically. Second, Dresselhaus effect is as important as the Rashba effect in semiconductor, more and more research focus on the effect of Dresselhaus

linear and cubic term but there are still some interesting issues worth to be studied. For example, the energy spectrum of the DSO quantum ring has mixing degeneracy states which was discussed first by G.E.Marques et al. in 2008 [3], but in their research, there are still many physical origins should be made clear step by step. In order to concentrate on the Dresselhaus spin-orbit interaction, we will not include other intrinsic and extrinsic SOI. Neglecting Rashba-type SOI is justified in a symmetric quantum well. In our results, we will present detail about solving coupling Hamiltonians to get degeneracy spectrum to Dresselhaus strength and discuss the particle density, spin accumulation and persistent charge current.

1.1   Spin-orbit coupling in solid state systems

Recently, more researches concentrate on the study of creating spintronic devices in semiconductor without magnetic materials which are designed by the interaction between spin-orbit coupling and quantum confinement. It can be realized by the spin-orbit interaction (SOI) to control electron spins. Datta and Das proposed an efficient model of spin-transistor in which the electron spin can transport and precess via SOI from a ferromagnetic source injecting into semiconductor to reaching a ferromagnetic drain [4]. The system is shown in Fig. 1.1. In this kind of spin-transistor, we can detect the polarization of the electron spin which depends on the strength of spin-orbit coupling by tuning an applying gate voltage. Besides, the spin polarization parallel to the polarization of the drain can pass through the channel, therefore, one can tune the voltage to modulate the current flow for 'on-' or 'off-' state.

Before we concentrate on the spintronics devices in semiconductor, we should understand the physical phenomenon clearly in nanoscale especially. Electron spin, the only internal degree of freedom of electrons, follows naturally from the Dirac equation when Dirac tried to put wave function in a covariant form, when space and time appear on equal footing. A nonrelativistic limit of the Dirac equation gives rise to the spin-orbit
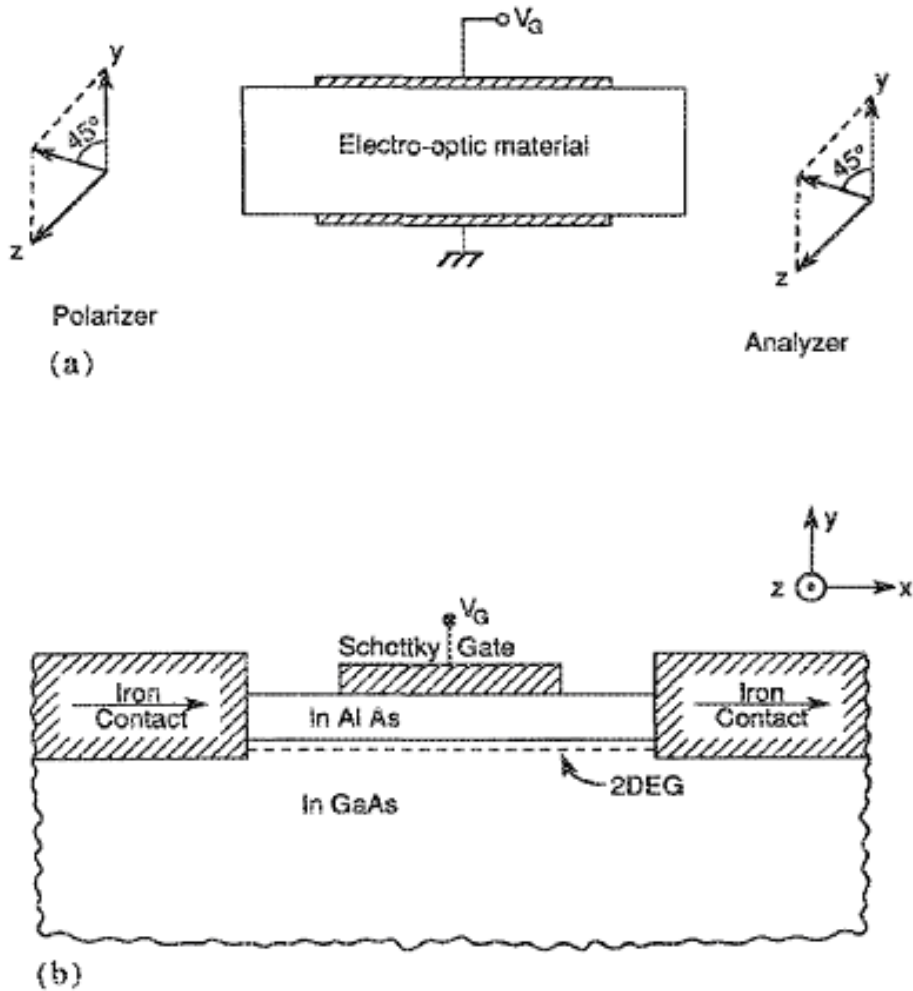
Figure 1.1: (a) Electro-optic light modulator. The polarizer makes the input light polarized at an angle of 45o with respect to the y axis; (b) Spin-polarized FET proposed by Datta et al. [4] in 1990. The iron contacts playing the roles of polarizer and analyzer are made of ferromagnetic materials. These figures were plotted by Datta et al. [4] in 1990.

interaction term, a term that has found great success in atomic energy spectra. The form of this spin-orbit interaction, in vacuum, is [5]

$$H_{so} = -\frac{e\hbar}{4m_0^2 c^2}\sigma \cdot (E \times p) = \frac{\hbar}{4m_0^2 c^2}\sigma \cdot (\nabla V \times p) \tag{1.1}$$

where m_0 is the free electron mass, $\hbar$ is the Planck constant and c is the velocity of light. The physical interpretation of H_{so} is given below. An electron moving in an electric potential region sees, in its frame of reference, an effective magnetic field couples with the electron spin through the magnetic moment of the electron spin. Therefore, the SOI is established via this effective magnetic field which depends on the orbital motion of the electron, and this physics holds in semiconductor too when $V(r)$ becomes the periodic potential of the host lattice and also the impurities.

The $k \cdot p$ model is the well-known method to describe electronic state calculations in semiconductor, when we investigate physical effect in the vicinity of the band edges. Furthermore, within the envelope function approximation (EFA), the energy band can be characterized by effective masses. The SOI in semiconductors requires, first of all, an effective electric field in the material. Such effective electric field can find contribution from the build-in crystal field when the crystal has bulk inversion asymmetric (BIA) the so-called Dresselhaus SOI [2], or structural inversion asymmetry (SIA), the so-called Rashba SOI [1]. The BIA is found in zincblende structure and the SIA in asymmetric quantum wells (QWs) or heterostructures.

However within the effective mass approximation, the effect of all the fast-varying atomic potential has been incorporated into the effective mass. Slower varying $V(r)$, with variation length scale much greater than the lattice spacing, is found to contribute to SOI with a much greater SO coupling constant λ. For a central potential $V(r)$ depends on only r without angular dependence in vacuum, the SO coupling is

4

$$\frac{\hbar}{4m_0^2c^2}\sigma\cdot(\nabla V\times p)=\frac{\hbar}{4m_0^2c^2}\frac{1}{r}\frac{dV}{dr}\sigma\cdot(r\times p)=\frac{\hbar^2}{4m_0^2c^2}\frac{1}{r}\frac{dV}{dr}\frac{L}{\hbar}\cdot\sigma=-\frac{\lambda_{vac}}{\hbar}\frac{1}{r}\frac{dV}{dr}L\cdot\sigma \quad (1.2)$$

where L is the orbital angular momentum,$\lambda_{vac}=-\hbar^2/(4m_0^2c^2)\approx-3.72\times10^{-6}\mathring{A}^2$.

But in a semiconductor, also for a central potential, the SO coupling can be expressed in the form of

$$H_{so}=-\frac{\lambda}{\hbar}\frac{1}{r}\frac{dV}{dr}L\cdot\sigma \qquad (1.3)$$

, where $\lambda\approx\frac{p^2}{3}\left[\frac{1}{E_g^2}-\frac{1}{(E_g+\Delta_0)^2}\right]$.

For a 2DEG, the SOI becomes $H_{so}=-\frac{\lambda}{\hbar}\frac{1}{\rho}\frac{dV(\rho)}{d\rho}L_z\cdot\sigma_z$. Here P is the momentum matrix element between s- and p-orbital, $E_g$is the energy band gap, and Δ_0 represents the SOI energy split to the spin split-off hole band [**?**]. Of particular interest is that $\lambda=120\mathring{A}^2$ in InAs, which is seven order of magnitude greater than λ_{vac} [6].

Roughly speaking, this large enhancement of SO coupling constant can be understood in the following. With $\lambda_{vac}\propto\frac{1}{m_0^2c^2}=\frac{1}{m_0}\frac{1}{m_0c^2}$, we can see that $\frac{\lambda}{\lambda_{vac}}\sim\frac{m_0}{m^*}\frac{m_0c^2}{E_g}$. For InAs, $\frac{m_0}{m^*}\sim\frac{1}{0.023};\frac{m_0c^2}{E_g}\sim\frac{0.5MeV}{0.418eV}$;leading to $\frac{\lambda}{\lambda_{vac}}\sim52\times10^6$. Comparing to, we see that the above hand waving argument has captured the essential physical origin of the great enhancement.

1.2 Introduction to persistent current

1.2.1 One-dimension ring with an external magnetic flux

In 1983, Buttiker et al. proposed a model [7] which is a one-dimensional normal mental ring threaded by a flux with elastic scattering at zero temperature. In this case, the single-electron states of this ring can be acquired from the band structure with the potential $V(x)=V(x+L)$, which the potential $V(x)$ around the loop with perimeter L
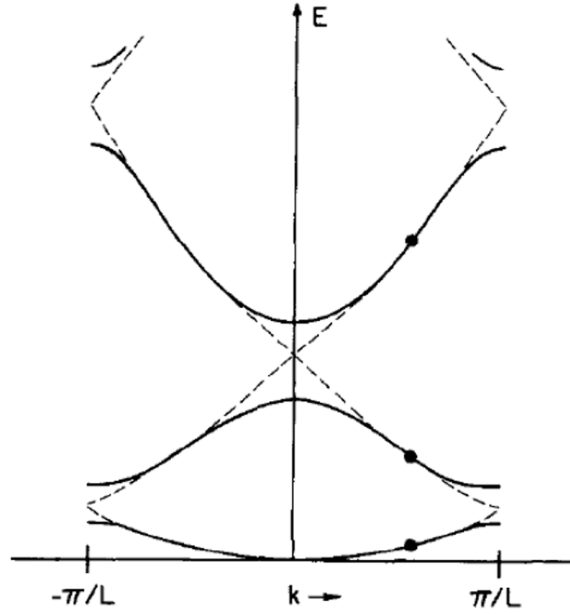
Figure 1.2: Band structure of a linear lattice with lattice constant L. The figure was obtained from Kronig-Penney model. [8]

corresponds to the time-varying vector potential of the system. The physical behavior of an electron passing through is the same as an electron in a linear lattice with periodic potential. The potential variation in one period is consistent with the change of the vector potential in one route around the ring.

We can see a similar phenomenon in Kronig-Penney model.[8] The band structure of a linear lattice with lattice constant L is shown in Fig. 1.2. The single-electron energy state of the ring system is an analogy of the band structure through the rule $\frac{\Phi}{\Phi_0} = -\frac{k}{(2\pi/L)}$, where the electron flux quantum $\Phi_0 = hc/e$. The electronic energy states $E_n(\Phi)$ periodic in flux Φ with period Φ_0 are shown in Fig. 1.3. The same periodic behavior occurs in the persistent current.

As we known, the current carried by each state $E_n(\Phi)$ for a time-independent flux at zero temperature is $i_n = -\frac{e}{L}\left[\frac{1}{\hbar}\frac{\partial E_n}{\partial k}\right]$. According to the analogy between the wave vector and magnetic flux, the current is obtained as $i_n = -c\frac{\partial E_n(\Phi)}{\partial \Phi}$. Then the total persistent charge current $I = \sum_n i_n = -c\sum_n \frac{\partial E_n(\Phi)}{\partial \Phi}$ can be obtained by summing over all occupied
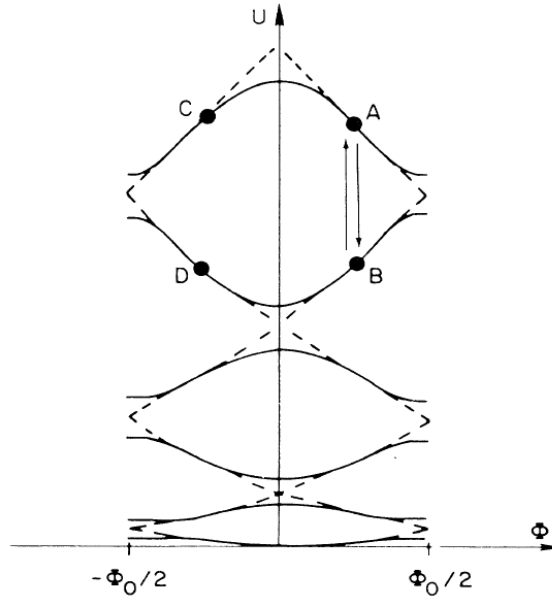
Figure 1.3: The single-electron energy state $E_n(\Phi)$ of the normal mental one-dimensional ring as a function of flux proposed by Buttiker et al.[9]

states up to the Fermi energy at zero temperature.

If the flux is time-dependent and increases linearly with time, there exists induced electric field $E = \frac{V}{L} = -\frac{1}{cL}\frac{d\Phi}{dt}$ coercing the state through the Brillouin zone [9]. Under this situation, we use the analogy between wave vector and magnetic flux again, and an electron will perform Bloch oscillation by circulating around the ring. The time for the electron to complete one cycle is $T = \frac{\Delta k}{(eE/\hbar)} = \frac{2\pi/L}{(eE/\hbar)} = \frac{2\pi\hbar}{eV}$ with $V = EL$. For one cycle, the variation of flux is equal to one flux quantum $\Phi_0 = hc/e$ corresponds to the change of wave vector equal to the reciprocal wave vector $G = 2\pi/L$. The electromotive field produces an oscillating current with frequency $\nu = eV/h$, i.e., a Josephson frequency with a single electronic charge. This persistent current will exist even when the field is turned off or the vector potential is fixed, and the current will keep at the value of flux to which it is fixed. [9]

1.2.2 Persistent current in mesoscopic rings with spin-orbit coupling

A mesoscopic ring system with spin-orbit coupling effect was discussed by Splettstosser et al. in 2003 [10]. The model is a mesoscopic isolated quasi-one-dimension ring with Rashba spin-orbit (RSO) coupling threaded by magnetic flux at low temperature. The external magnetic field provides a z-direction flux and the effective magnetic field coming from RSO coupling is in the radial r-direction. The tilt angle θ between z and r is presented as the strength of the RSO coupling shown in Fig. 1.4.

If the particle number is not too large, the effect of RSO coupling on persistent charge current with even number or odd number of electrons is quite different from each other. In the other way, the prominent effect of RSO coupling on persistent spin current is the existence of the spin current for even electron number in the ring which vanishes in the absence of RSO coupling.

The energy spectrum for the ring with an idealized impurity was obtained by Splettstosser et al. and shown in Fig. 1.5. The author expressed the impurity by a delta-function barrier $V_0 \delta (\phi)$ and the Zeeman energy is negligible in the local spin frame. They demonstrated the energy spectrum from the Hamiltonian of electrons in x-y plane. The electrons are assumed to move in a ring confined by a parabolic radial potential $V_c (r) = \frac{1}{2} m \omega^2 (r - a)^2$ in the Hamiltonian:

$$H = \frac{(p - eA)_x^2 + (p - eA)_y^2}{2m} + V_c (r) + H_{so} = H_0 + H_{so} \tag{1.4}$$

where $H_{so} = \frac{\alpha}{\hbar} \left[\sigma_x (p - eA)_y - \sigma_y (p - eA)_x \right]$ is the Rashba spin-orbit coupling term.

Briefly speaking, the author obtained the approximated secular equation of the system by projecting the Hamiltonian on the eigenstates of the Hamiltonian without RSO coupling term and modeling the impurity by its energy-dependent transmission amplitude. Then they solved the secular equation to get the energy spectrum. When comparing with
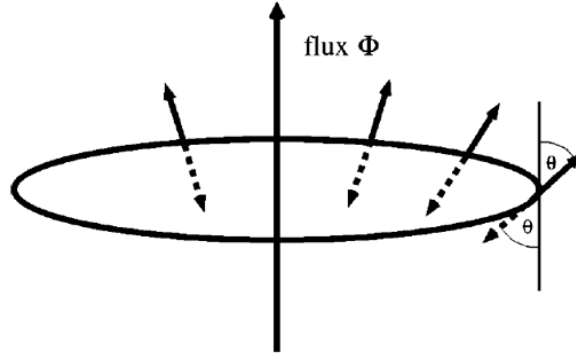
Figure 1.4: A mesoscopic ring with Rashba spin-orbit coupling threaded by magnetic flux. The external magnetic flux is in z-direction and the angle θ between z and r parameterizes the strength of the RSO coupling. This figure was plotted by Splettstosser et al. in 2003. [10]
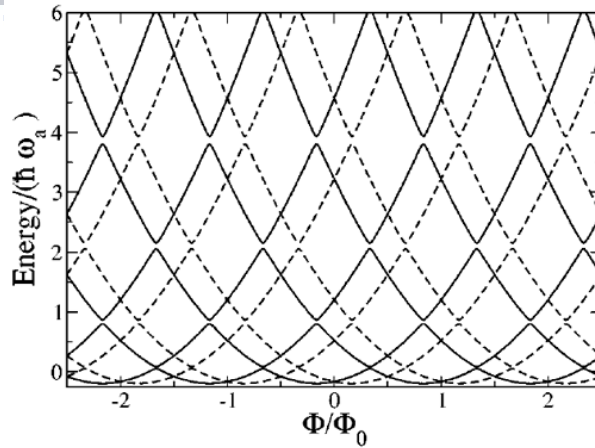
Figure 1.5: It is the energy spectrum for the ideal one-dimension ring with a delta-barrier impurity. Parameters are impurity strength constant $A = 0.1$ and title angle $\cos\theta = 2/5$. The energy levels are shifted in flux direction by $1/\cos\theta$. Solid lines correspond to spin-up states in the local spin-frame basis while dashed line to spin-down states. This figure was plotted by Splettstosser et al. in 2003. [10]

the energy levels after calculation for the same ring without RSO coupling, we can find that the energy levels for the system with RSO coupling are shifted in the flux direction by $1/\cos\theta$. For the reason of the energy splitting coming from RSO coupling, $1/\cos\theta$ corresponds to the strength of the coupling. The shift in flux direction is different by the electron spin polarization state. On the basis of local spin frame, spin-up states move to the left (solid line) while spin-down state to the right (dash line).

At zero temperature, the persistent charge current carried by each state n is $i_n = -\frac{\partial E_n(\Phi)}{\partial\Phi}$, and n stands for a set of quantum numbers used to label the eigenstates including the spin projection in the local spin frame. Therefore, the total persistent charge current I is obtained by summing over all occupied states, i.e., $I = \sum\limits_{n=occupied} i_n = -\frac{\partial E_{gs}}{\partial\Phi}$, where E_{gs} is the ground state energy of the system.

The flux dependence of the persistent charge current is individually different according to the number of electrons N_e. Here three cases are discussed for N_e is not too large:(i)$N_e = 4N$, (ii) $N_e = 4N + 2$, and (iii)$N_e = 2N + 1$ where N is a positive integer. If N_e is large enough, the persistent charge current has a general behavior independent of N_e.

In case (i), where $N_e = 4N$, the numbers of spin-up and spin-down electrons are both even. The current flux characteristics are shown in Fig. 1.6. The solid line is for the system in the absence of RSO coupling. The effect of RSO coupling on the charge current is getting more obvious as $1/\cos\theta$ increases. For each spin polarization, the current-characteristics of even number spin electrons are shifted in flux by $\pm 1/2\cos\theta$. The total persistent charge current of the system is the superposition of the two shifted current flux characteristics.

Case (ii), where $N_e = 4N + 2$, is obtained from the 4N case by shifting flux by $\Phi_0/2$ and corresponds to an odd number of spin-up and spin-down electrons. The current is the analogous superposition of the two shifted current flux characteristics for odd number spin electrons. In these two case (i) and (ii), the strength of RSO coupling corresponding to $1/\cos\theta$ can be measured. Further more, we can observe the behavior that the minimum
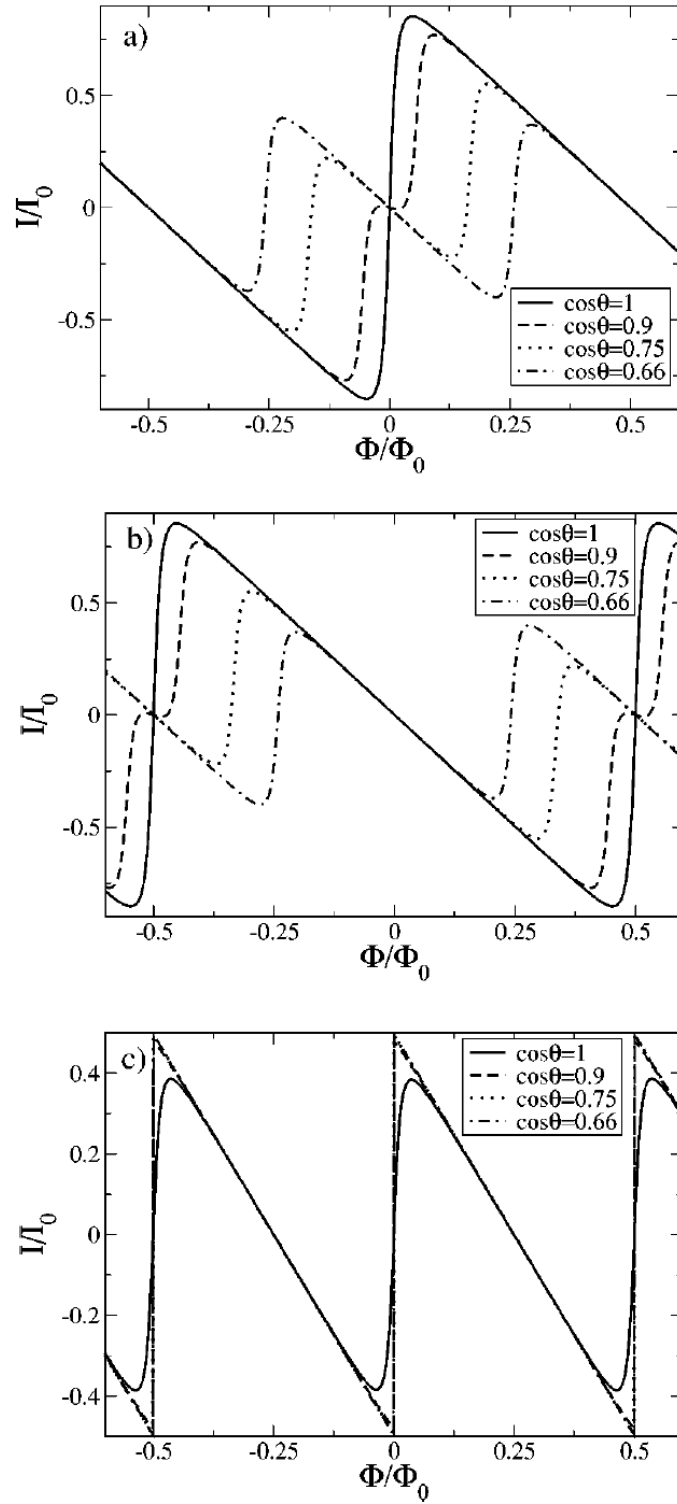
Figure 1.6: Persistent charge current-flux characteristics for a set of values for the spin-orbit coupling strength. The total number of electrons is $4N$ in panel (a). $4N+2$ in panel (b), and $2N+1$ in panel (c) with the impurity strength constant A=0.1. These figures were plotted by Splettstosser et al. in 2003. [10]

distance between two jumps of the current within one period interval is related to $1/\cos\theta$.

For case (iii), $N_e = 2N + 1$. As strength of RSO coupling $1/\cos\theta$ increases, the coupling suppresses the rounding more. It is because that the rounding comes from the impurity, RSO plays a role of decreasing the effect of impurity. This suppression makes the current flux characteristics from sawtooth shapes with jumps. This jumps come from the level crossing in the energy for the system with opposite spin in this odd number of electrons.

The persistent spin current of each eigenstate (q, σ) in the quantization axis of local spin frame is $I_\theta^{(q\sigma)} = -\frac{1}{e}\frac{\partial E_{q,\sigma}}{\partial \Phi}$, where $E_{q,\sigma}$ is an eigenenergy of local spin frame. The eigenstates of the system in the local spin frame are $e^{i(q+1/2)\phi}\left|\pm\right\rangle$ with $\left|\pm\right\rangle$ denoting the eigenspinors of spin operator $\widehat{\sigma}_z$ and q being an integer. This spin current for each state is the charge current for each state multiplied by the magnetization over charge e factor where the total spin current is obtained by summing the contribution from each state like the case in charge current $I_\theta = \sum_{q\sigma} I_\theta^{(q\sigma)}$ at zero temperature. This spin current is the projection onto the quantization axis of local spin frame. The other projections of spin current can be derived from I_θ through $I_z = I_\theta \cos\theta$ and $I_r = I_\theta \sin\theta$, where I_z is for z projection and I_r is for the radial r projection.

For even number electrons $4N + 2$, the effect of RSO coupling on the persistent spin current can be observed through comparison of the spin current with the charge current. In this ring for even number of electrons, the spin current vanishes without RSO coupling. However, with RSO coupling, the spin current of the ring with electrons $4N + 2$ is shown with dashed line in Fig. 1.7. by Splettstoesser et al. [10]. Evidently, the spin current has nonzero value at zero temperature and its characteristic curve exhibits dramatically different flux dependence from the charge characteristic curve (solid line) of the same ring. It shows a clear signature of RSO coupling. The RSO coupling produces a relative shift of energy band in flux direction and hence enables a finite persistent spin current for an even number of electrons.

For odd number of electrons $(2N + 1)$, the spin current is supposed to be proportional
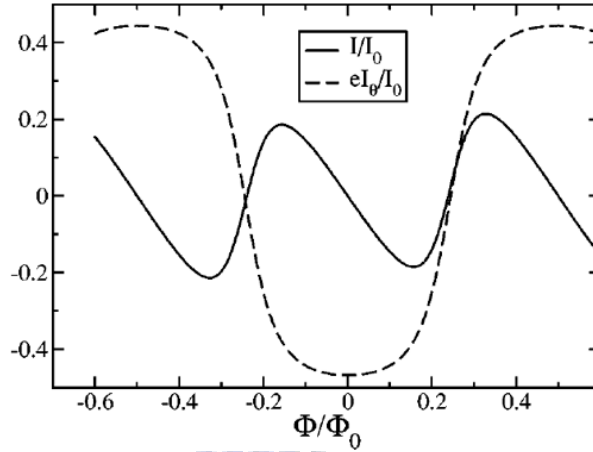
Figure 1.7: In even number electrons $4N + 2$ case, comparison of the persistent spin current (dash line) with the charge current (solid line) of the ring. The spin current is for spin projection onto the local spin frame and parameters are the impurity strength constant $A = 0.5$, the tilt angle $\cos\theta = 0.66$. This figure was plotted by Splettstosser et al. in 2003. [10]
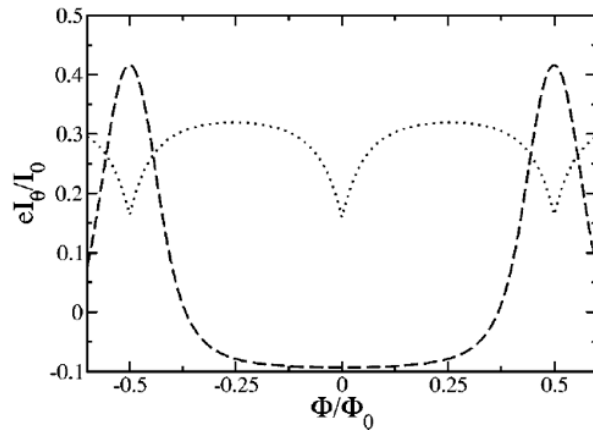
Figure 1.8: Persistent spin currents of the ring with odd number electrons $2N + 1$ (dotted line) and even number electrons $4N + 2$ (dashed line). Parameters are impurity strength constant $A = 0.5$ and tilt angle $\cos\theta = 0.9$ corresponding to a small spin-orbit coupling strength. The figure was plotted by Splettstoesser et al. [10]

the charge current in the absence RSO coupling. In this ring with RSO coupling, the spin current of the ring with odd number electrons is shown with dotted curve in Fig. 1.8. The spin current flux characteristic curve has different flux dependence from the charge characteristic curve. According to the result, the proportion relation does not exist because of the presence of RSO coupling.

The persistent spin current just like a magnetization current, could be detectable via tuning an external electric field. By making a Lorentz transform to the rest frame of spin, the electrostatic potential for a point at a distance z is obtained as $\varphi\left(z\right) \approx \frac{\mu_0}{4\pi}g\mu_B I_\theta \sin\theta \frac{a}{z^2}$. Where the distance z is the vertical length from the center of the ring and is summed to be much smaller than the radius a of the ring. Besides, in the expression of potential, g is the gyromagnetic ratio, μ_0 is the vacuum permeability, and μ_B is the Bohr magneton. This potential expression is the same as the one resulting from the persistent spin current in Heisenberg rings derived by Kopietz et al. [11]. If it is possible to measure the spin current through electric field generated by its transported magnetization, the existence and magnitude of RSO coupling in conducting rings can be finally verified.

Chapter 2

Finite width mesoscopic Dresselhaus spin-orbit (DSO) ring

Recently, it is possible to grow self-assembled annulus semiconductor structures in a large range of inner and outer radii by using molecular beam epitaxy. Typical samples show a circular cross section with an inner radius about 10 nm, and the outer radius ranges between 30 and 70 nm [12–16]. This kind of structures has been studied by their potential applications as spintronic and quantum computing. [14, 15, 17, 18]. In this chapter, we will start the system from the Hamiltonian to get the energy spectrum and spin density.

2.1 Model of a mesoscopic ring with Dresselhaus spin-orbit coupling

2.1.1 Hamiltonian

The geometric model is an isolated finite width mesoscopic ring with Dresselhaus spin-orbit (DSO) coupling without any external electromagnetic field. The cross section of the structure is shown in Fig. 2.1. Assuming r_1 (r_2) and d are the inner (outer) radii and height, the center of the ring is at origin.
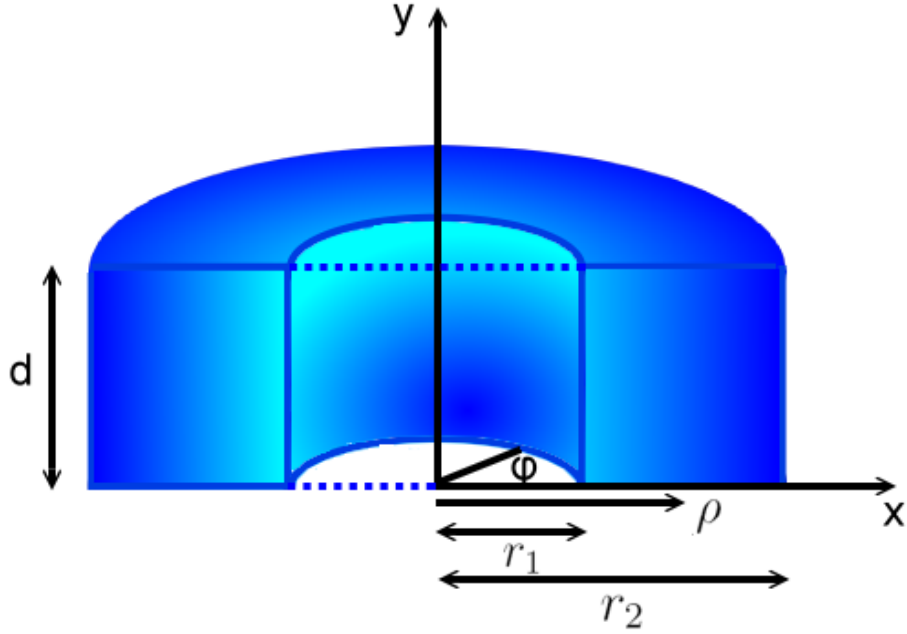
Figure 2.1: The figure is the cross section of the finite width mesoscopic ring, where r_1 and r_2 are the inner and outer radii.

The total single-particle Hamiltonian in a mesoscopic ring that has bulk inversion asymmetry (BIA) and formed out of a quantum well with the well thickness along z and z along [001] has the form:

$$H = H_0 + H_{DSO} \tag{2.1}$$

$$H_0 = \frac{p^2}{2m^*} + V(\overrightarrow{\rho}, z) \tag{2.2}$$

$$H_{DSO} = \overrightarrow{\sigma} \cdot \overrightarrow{h}_{\overrightarrow{k}}. \tag{2.3}$$

Here $\overrightarrow{h}_{\overrightarrow{k}}$ denotes the effective magnetic field arising from the DSO coupling, m^* is the electron effective mass, $V(\overrightarrow{\rho}, z)$ is a hard-wall confinement potential, β is the Dresselhaus SO coupling constant, and $\overrightarrow{\sigma} = (\sigma_x, \sigma_y, \sigma_z)$ is the vector of Pauli spin matrices. For the case of a narrow quantum well, the electrons occupy only the lowest subband, we can average $\overrightarrow{h}_{\overrightarrow{k}}$ over the well thickness d to give

$$h_k^x = \beta k_x \left(k_y^2 - \langle k_z^2 \rangle \right), \tag{2.4}$$

$$h_k^y = \beta k_y \left(\langle k_z^2 \rangle - k_x^2 \right), \tag{2.5}$$

$$h_k^z = \beta \langle k_z \rangle \left(k_x^2 - k_y^2 \right) \cong 0, \tag{2.6}$$

$$\langle k_z \rangle = 0, \tag{2.7}$$

$$\langle k_z^2 \rangle \cong \left(\frac{\pi}{d} \right)^2. \tag{2.8}$$

If we just consider the k-linear BIA contribution, the effective H_{DSO} assumes the form

$$H_{DSO} = H_{1D} = \beta \langle k_z^2 \rangle \left[\sigma_y k_y - \sigma_x k_x \right] = -\beta \langle k_z^2 \rangle \left[\sigma_+ k_+ + \sigma_- k_- \right], \tag{2.9}$$

where $\sigma_\pm = \frac{1}{2} \left(\sigma_x \pm i\sigma_y \right)$ and $k_\pm = k_x \pm ik_y$. The effect of the operator $\sigma_\pm$ with subscript $+ (-)$ is to increase (decrease) the spin of the electron by unit of $\hbar$. The operator $k_\pm$ can be expressed in the form $k_\pm = -ie^{\pm i\varphi} \left[\frac{\partial}{\partial \rho} \pm i\frac{1}{\rho}\frac{\partial}{\partial \varphi} \right] \equiv -ie^{\pm i\varphi} p_{\rho,\varphi}^\pm$ which effect is to change the orbital angular momentum by $\pm\hbar$. This is evident by the factor $e^{\pm i\phi}$ in $k_\pm$.

In matrix form

$$H \cong \begin{pmatrix} \frac{p^2}{2m^*} + V & -\beta < k_z^2 > k_+ \\ -\beta < k_z^2 > k_- & \frac{p^2}{2m^*} + V \end{pmatrix} = \begin{pmatrix} \frac{p^2}{2m^*} + V & i\beta(\frac{\pi}{d})^2 e^{i\varphi} p_{\rho,\varphi}^+ \\ i\beta(\frac{\pi}{d})^2 e^{-i\varphi} p_{\rho,\varphi}^- & \frac{p^2}{2m^*} + V \end{pmatrix}. \tag{2.10}$$

In the following, we will guess the form of the eigenstate of H with the choice of quantum numbers parallel that of the unperturbed eigenstate $\left| E_{n,m,\sigma}^0 \right\rangle$. Here n, m, σ are, respectively, the quantum numbers for the radial, azimuthal and spin degrees of freedom. Hints for the form of the eigenstate of H can be obtained from applying H_{DSO} repeatedly upon $\left| E_{n,m,\sigma}^0 \right\rangle$.

Consider, for example, applying H_{DSO} to $\left|E^0_{n,m,\uparrow}\right\rangle$, we get, apart from a proportionality constant $-\beta\left\langle k_z^2\right\rangle$, the essence of H_{DSO} is carried by the operator $\sigma_+k_+ + \sigma_-k_-$,

$$
\begin{aligned}
H_{DSO}\left|E^0_{n,m,\uparrow}\right\rangle &\propto (\sigma_+k_+ + \sigma_-k_-)\left|E^0_{n,m,\uparrow}\right\rangle \\
&= \sigma_-k_-\left|E^0_{n,m,\uparrow}\right\rangle \\
&\propto \left|E^{(1)}_{n,m-1,\downarrow}\right\rangle,
\end{aligned}
\tag{2.11}
$$

where the superscript (1) denotes the state $\left|E^{(1)}_{n,m,\sigma}\right\rangle$ to have a different radial dependence from that of $\left|E^0_{n,m,\sigma}\right\rangle$. Applying H_{DSO} the second time gives

$$
\begin{aligned}
H_{DSO}\left|E^{(1)}_{n,m-1,\downarrow}\right\rangle &\propto (\sigma_+k_+ + \sigma_-k_-)\left|E^{(1)}_{n,m-1,\downarrow}\right\rangle \\
&= \sigma_+k_+\left|E^{(1)}_{n,m-1,\downarrow}\right\rangle \\
&\propto \left|E^{(2)}_{n,m,\uparrow}\right\rangle.
\end{aligned}
\tag{2.12}
$$

From this we see that only $|E_{n,m,\uparrow}\rangle$ and $|E_{n,m-1,\downarrow}\rangle$ are coupled by the action of H_{DSO}. We no longer use the superscript in the states $|E_{n,m,\sigma}\rangle$ because the eigenstate of H should include arbitrary number of times the H_{DSO} is applied. This amounts to give the form for the total eigenfunction where $f_1(\rho)$, $f_2(\rho)$ have to be solved explicitly.

$$
\Psi = \begin{pmatrix} f_1(\rho)e^{im\varphi} \\ f_2(\rho)e^{i(m-1)\varphi} \end{pmatrix}
\tag{2.13}
$$

For a hard-wall confinement potential

$$
V(\overrightarrow{\rho},z) = \begin{cases} 0 & \text{for } r_1 < \rho < r_2 \text{ and } |z| < \frac{d}{2} \\ \infty & \text{otherwise} \end{cases}
\tag{2.14}
$$

the Schrodinger equations inside the ring is given by

$$
\begin{pmatrix} \frac{p^2}{2m^*} & i\beta(\frac{\pi}{d})^2 e^{i\varphi}p_{\rho,\varphi}^+ \\ i\beta(\frac{\pi}{d})^2 e^{-i\varphi}p_{\rho,\varphi}^- & \frac{p^2}{2m^*} \end{pmatrix} \begin{pmatrix} f_1(\rho)e^{im\varphi} \\ f_2(\rho)e^{i(m-1)\varphi} \end{pmatrix} = E \begin{pmatrix} f_1(\rho)e^{im\varphi} \\ f_2(\rho)e^{i(m-1)\varphi} \end{pmatrix}.
\tag{2.15}
$$

2.1.2 Dimensionless

In order to get more clearly formula and prepare for the Numerical analysis, we set some parameters to dimensionless the Hamiltonian: (a) Fermi wave length l_f, (b) Fermi wave vector $k_f = \frac{1}{l_f}$, (c) Fermi energy $E_f = \frac{\hbar^2 k_f^2}{2m^*}$, (d) Del operator in polar coordinates $\nabla = k_f \widetilde{\nabla}$, (e) $p_{\rho,\varphi}^\pm = k_f \widetilde{p}_{\rho,\varphi}^\pm$, (f) $\widetilde{E} = \frac{E}{E_f}$, (g) $\widetilde{\beta} = \frac{\beta \left(\frac{\pi}{d}\right)^2 \cdot k_f}{E_f}$, (h) $\widetilde{\rho}_r = \frac{\rho}{r_1}$.

After calculation, we get the dimensionless couple equations (The detail process is shown in Appendix A).

$$
\begin{cases}
\widetilde{\nabla}^2 \left[f_1(\widetilde{\rho}_r)e^{im\varphi}\right] - i\widetilde{\beta}e^{im\varphi}\left[\frac{\partial}{\partial\widetilde{\rho}}f_2(\widetilde{\rho}_r) - \frac{(m-1)}{\widetilde{\rho}}f_2(\widetilde{\rho}_r)\right] = -\widetilde{E}f_1(\widetilde{\rho}_r)e^{im\varphi} \\
\widetilde{\nabla}^2 \left[f_2(\widetilde{\rho}_r)e^{i(m-1)\varphi}\right] - i\widetilde{\beta}e^{i(m-1)\varphi}\left[\frac{\partial}{\partial\widetilde{\rho}}f_1(\widetilde{\rho}_r) + \frac{m}{\widetilde{\rho}}f_1(\widetilde{\rho}_r)\right] = -\widetilde{E}f_2(\widetilde{\rho}_r)e^{i(m-1)\varphi}
\end{cases}
\tag{2.16}
$$

Since these differential equations have the forms of Bessel equation and the recurrence relation, we can choose the Bessel functions as the spinor part eigenfunctions. Therefore,

$$
\begin{cases}
-\gamma^2 A J_m(\gamma\widetilde{\rho}_r)e^{im\varphi} - i\widetilde{\beta}\left[-\gamma B J_m(\gamma\widetilde{\rho}_r)\right]e^{im\varphi} = -\widetilde{E}A J_m(\gamma\widetilde{\rho}_r)e^{im\varphi} \\
-\gamma^2 B J_{m-1}(\gamma\widetilde{\rho}_r)e^{i(m-1)\varphi} - i\widetilde{\beta}\left[\gamma A J_{m-1}(\gamma\widetilde{\rho}_r)\right]e^{i(m-1)\varphi} = -\widetilde{E}B J_{m-1}(\gamma\widetilde{\rho}_r)e^{i(m-1)\varphi}
\end{cases}
\tag{2.17}
$$

where A and B are the coefficients of the two eigenfunction components.

Comparing with above couple equations, we find that the ratio of the coefficients $R = \frac{B}{A} = \pm i$, then we get two branches of wave functions

$$
\Psi = \begin{pmatrix} J_m(\gamma\widetilde{\rho}_r)e^{im\varphi} \\ i J_{m-1}(\gamma\widetilde{\rho}_r)e^{i(m-1)\varphi} \end{pmatrix}, \Psi = \begin{pmatrix} J_m(\gamma\widetilde{\rho}_r)e^{im\varphi} \\ -i J_{m-1}(\gamma\widetilde{\rho}_r)e^{i(m-1)\varphi} \end{pmatrix}.
\tag{2.18}
$$

2.1.3 Eigenenergy and Eigenstate

We get two energy dispersion $\gamma^2 + \widetilde{\beta}\gamma - \widetilde{E} = 0$ and $\gamma^2 - \widetilde{\beta}\gamma - \widetilde{E} = 0$ when R is equal to $+i$ and $-i$ respectively. Then, if we set $\gamma_1 = \frac{1}{2}\left(\widetilde{\beta} + \sqrt{\widetilde{\beta}^2 + 4\widetilde{E}}\right)$ and $\gamma_2 = \frac{1}{2}\left(-\widetilde{\beta} + \sqrt{\widetilde{\beta}^2 + 4\widetilde{E}}\right)$, we can obtain four-eigenstates (first kind of Bessel function):

$$
(I)\begin{pmatrix} J_m\left(\gamma_1\widetilde{\rho}_r\right)e^{im\varphi} \\ -iJ_{m-1}\left(\gamma_1\widetilde{\rho}_r\right)e^{i(m-1)\varphi} \end{pmatrix}, (II)\begin{pmatrix} J_m\left(-\gamma_1\widetilde{\rho}_r\right)e^{im\varphi} \\ iJ_{m-1}\left(-\gamma_1\widetilde{\rho}_r\right)e^{i(m-1)\varphi} \end{pmatrix},
$$
$$
(III)\begin{pmatrix} J_m\left(\gamma_2\widetilde{\rho}_r\right)e^{im\varphi} \\ iJ_{m-1}\left(\gamma_2\widetilde{\rho}_r\right)e^{i(m-1)\varphi} \end{pmatrix}, (IV)\begin{pmatrix} J_m\left(-\gamma_2\widetilde{\rho}_r\right)e^{im\varphi} \\ -iJ_{m-1}\left(-\gamma_2\widetilde{\rho}_r\right)e^{i(m-1)\varphi} \end{pmatrix}. \tag{2.19}
$$

But (I) (II) and (III) (IV) have the same forms, there are just two independent bases. Therefore, we chose (I) and (III) to be our eigenstates. Besides, the index of m should be integers (including positive and negative), then we have to introduce the second kind of Bessel function "Neumann" to be eigenstates.

$$
(I)\begin{pmatrix} N_m\left(\gamma_1\widetilde{\rho}_r\right)e^{im\varphi} \\ -iN_{m-1}\left(\gamma_1\widetilde{\rho}_r\right)e^{i(m-1)\varphi} \end{pmatrix}, (II)\begin{pmatrix} N_m\left(-\gamma_1\widetilde{\rho}_r\right)e^{im\varphi} \\ iN_{m-1}\left(-\gamma_1\widetilde{\rho}_r\right)e^{i(m-1)\varphi} \end{pmatrix},
$$
$$
(III)\begin{pmatrix} N_m\left(\gamma_2\widetilde{\rho}_r\right)e^{im\varphi} \\ iN_{m-1}\left(\gamma_2\widetilde{\rho}_r\right)e^{i(m-1)\varphi} \end{pmatrix}, (IV)\begin{pmatrix} N_m\left(-\gamma_2\widetilde{\rho}_r\right)e^{im\varphi} \\ -iN_{m-1}\left(-\gamma_2\widetilde{\rho}_r\right)e^{i(m-1)\varphi} \end{pmatrix}. \tag{2.20}
$$

In order to get more clear physical meaning, we change Bessel functions to Hankel functions: $H_\alpha^{(1)}(x) = J_\alpha(x) + iN_\alpha(x)$, $H_\alpha^{(2)}(x) = J_\alpha(x) - iN_\alpha(x)$. Thus, we get the total eigenfunction:

$$
\Psi = a\begin{pmatrix} H_m^{(1)}\left(\gamma_1\widetilde{\rho}_r\right)e^{im\varphi} \\ -iH_{m-1}^{(1)}\left(\gamma_1\widetilde{\rho}_r\right)e^{i(m-1)\varphi} \end{pmatrix} + b\begin{pmatrix} H_m^{(2)}\left(\gamma_1\widetilde{\rho}_r\right)e^{im\varphi} \\ -iH_{m-1}^{(2)}\left(\gamma_1\widetilde{\rho}_r\right)e^{i(m-1)\varphi} \end{pmatrix}
$$
$$
+ c\begin{pmatrix} H_m^{(1)}\left(\gamma_2\widetilde{\rho}_r\right)e^{im\varphi} \\ iH_{m-1}^{(1)}\left(\gamma_2\widetilde{\rho}_r\right)e^{i(m-1)\varphi} \end{pmatrix} + d\begin{pmatrix} H_m^{(2)}\left(\gamma_2\widetilde{\rho}_r\right)e^{im\varphi} \\ iH_{m-1}^{(2)}\left(\gamma_2\widetilde{\rho}_r\right)e^{i(m-1)\varphi} \end{pmatrix}, \tag{2.21}
$$

where a, b, c and d are the coefficients which can be decided by confinement potential and normalization.

Since the annulus is defined by the hard-wall confining potential Eq. (2.14), we can apply the boundary conditions $\Psi\left(\rho = r_1\right) = 0$, $\Psi\left(\rho = r_2\right) = 0$. These conditions give the equation set:

$$
\begin{pmatrix}
H_m^{(1)}\left(\gamma_1 r_1\right) & H_m^{(2)}\left(\gamma_1 r_1\right) & H_m^{(1)}\left(\gamma_2 r_1\right) & H_m^{(2)}\left(\gamma_2 r_1\right) \\
-H_{m-1}^{(1)}\left(\gamma_1 r_1\right) & -H_{m-1}^{(2)}\left(\gamma_1 r_1\right) & H_{m-1}^{(1)}\left(\gamma_2 r_1\right) & H_{m-1}^{(2)}\left(\gamma_2 r_1\right) \\
H_m^{(1)}\left(\gamma_1 r_2\right) & H_m^{(2)}\left(\gamma_1 r_2\right) & H_m^{(1)}\left(\gamma_2 r_2\right) & H_m^{(2)}\left(\gamma_2 r_2\right) \\
-H_{m-1}^{(1)}\left(\gamma_1 r_2\right) & -H_{m-1}^{(2)}\left(\gamma_1 r_2\right) & H_{m-1}^{(1)}\left(\gamma_2 r_2\right) & H_{m-1}^{(2)}\left(\gamma_2 r_2\right)
\end{pmatrix}
\begin{pmatrix} a \\ b \\ c \\ d \end{pmatrix} = 0 \quad (2.22)
$$

If there exists non-trivial solution for a, b, c and d, the determinant of the matrix M must vanish, i.e.,

$$
\det\left(M\right) = 0, \tag{2.23}
$$

where

$$
M = \begin{pmatrix}
H_m^{(1)}\left(\gamma_1 r_1\right) & H_m^{(2)}\left(\gamma_1 r_1\right) & H_m^{(1)}\left(\gamma_2 r_1\right) & H_m^{(2)}\left(\gamma_2 r_1\right) \\
-H_{m-1}^{(1)}\left(\gamma_1 r_1\right) & -H_{m-1}^{(2)}\left(\gamma_1 r_1\right) & H_{m-1}^{(1)}\left(\gamma_2 r_1\right) & H_{m-1}^{(2)}\left(\gamma_2 r_1\right) \\
H_m^{(1)}\left(\gamma_1 r_2\right) & H_m^{(2)}\left(\gamma_1 r_2\right) & H_m^{(1)}\left(\gamma_2 r_2\right) & H_m^{(2)}\left(\gamma_2 r_2\right) \\
-H_{m-1}^{(1)}\left(\gamma_1 r_2\right) & -H_{m-1}^{(2)}\left(\gamma_1 r_2\right) & H_{m-1}^{(1)}\left(\gamma_2 r_2\right) & H_{m-1}^{(2)}\left(\gamma_2 r_2\right)
\end{pmatrix}. \tag{2.24}
$$

The more detail process is shown in Appendix A.

2.2 Numerical results and discussion

2.2.1 Energy spectrum

Physical parameters used in the calculation are obtained for the case of GaAs: with DSO coupling constant $\beta = 25 eV \cdot \overset{o}{A}$, effective mass $m^* \approx 0.067 m_e$, Fermi wave length $\lambda_f = 40 nm$. Structures parameters are inner radius $r_1 = 10 nm$, outer radius $r_2 = 70 nm$ and the height of the ring $d = 50 \overset{o}{A}$. [3].

Fig. 2.2 presents the energy spectrum for the quantum ring which is determined from the determinant equation Eq. (2.23) and Eq. (2.24), where γ_1 and γ_2 contain the energy E. We want to show the effects caused by the DSOI on the first seven quantum ring energy levels in units of E_f, as a function of the dimensionless DSOI coupling constant $\widetilde{\beta}$. Due to the confinement potential and in the absence of the DSO interaction, we know that there exist discrete energy levels in y-axis. And each of them have degenerate states, namely, $\left|E^0_{n,\pm m,\uparrow}\right\rangle$ and $\left|E^0_{n,\pm m,\downarrow}\right\rangle$ for a given eigenenergy $E^0_{n,m,\sigma}$. When we introduce, however, the DSOI strength, we can see that the unperturbed energy level splitting into two parts and most of them decreasing as $\widetilde{\beta}$ increasing monotically. Specially, some eigenenergies have the trend which arise up first and then go down when $\widetilde{\beta}$ increasing.

In this section, we will focus on the physical insight of the splitting energy in our system. First, we propose a useful regulation to understand the development of the states. If we just consider the confinement potential in the quantum ring without DSOI, we can get the discrete quantum energy levels and each of them has different degeneracy states respectively, for instance, there are four degeneracy states $\left|E^0_{1,3,\uparrow}\right\rangle$, $\left|E^0_{1,3,\downarrow}\right\rangle$, $\left|E^0_{1,-3,\uparrow}\right\rangle$ and $\left|E^0_{1,-3,\downarrow}\right\rangle$ in the same eigenenergy $E^0_{1,\pm3}$. However, if we add the DSO interaction to our system, we find that each original degeneracy energy level split into two groups of energy levels, and the new energy level exists new degeneracy states which is the superposition of the original eigenstates in H_0. The phenomenon can be understood by the operator form of the $H_{DSO} = -\beta \langle k_z^2 \rangle (\sigma_+ k_+ + \sigma_- k_-)$ which has been presented in Eq. (2.11) to Eq. (2.12) in section 2.1. In H_{DSO}, the operators k_+ and k_- are like the angular moment
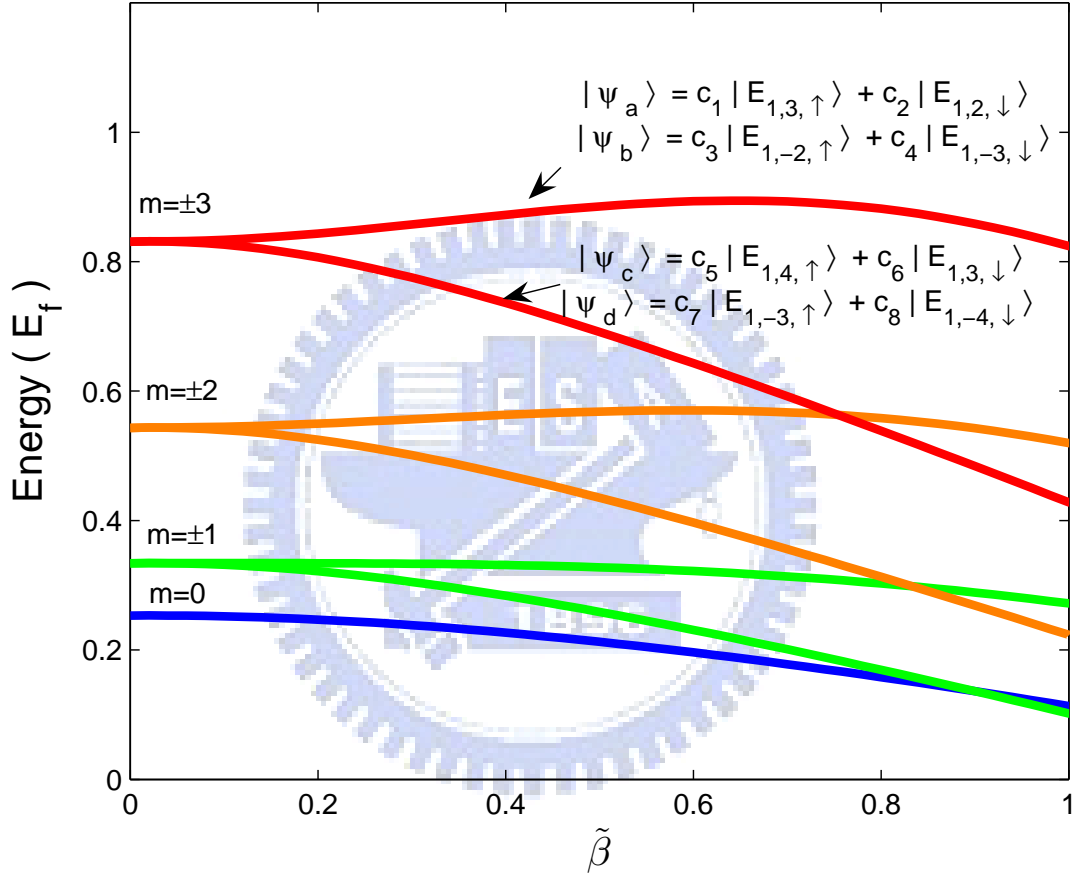
Figure 2.2: The energy spectrum for the quantum ring which is determined from the determinant equation Eq. (2.23) and Eq. (2.24), and it is shown the effects caused by the DSOI on the first seven quantum ring energy levels in units of E_f, as a function of the dimensionless DSO coupling constant $\widetilde{\beta}$. These doubly degeneracy states come from the superposition of the different unperturbed eigenstates respectively. The physical parameters are obtained for the case of GaAs: $\beta = 25eV \cdot \overset{o}{A}$, $m^* \approx 0.067m_e$, $\lambda_f = 40nm$, $r_1 = 10nm$, $r_2 = 70nm$, $d = 50 \overset{o}{A}$.

operator, the operators σ_+ and σ_- are like spinor operator. Each of them can create or destroy the quantum number m or $\uparrow\downarrow$ respectively. Today, we use H_{DSO} to operate the unperturbed states repeatedly in the quantum ring, the angular moment quantum number and the spin quantum number are created or destroyed respectively to become new superposition states $|\psi_a\rangle = c_1|E_{1,3,\uparrow}\rangle + c_2|E_{1,2,\uparrow}\rangle$, $|\psi_b\rangle = c_3|E_{1,-2,\uparrow}\rangle + c_4|E_{1,-3,\downarrow}\rangle$, $|\psi_c\rangle = c_5|E_{1,4,\uparrow}\rangle + c_6|E_{1,3,\downarrow}\rangle$ and $|\psi_d\rangle = c_7|E_{1,-3,\uparrow}\rangle + c_8|E_{1,-4,\downarrow}\rangle$. Therefore, we can use this simple method to understand the development of states in DSOI systems.

Second, we find that the relative weighting between the constituent bases state ket plays an important role to effect the trend of the energy spectrum when the DSOI strength increases slowly. For example, we start from the unperturbed energy level in $m = \pm 3$. We can understand that the probability of the states $|E_{1,3,\uparrow}\rangle$ and $|E_{1,-3,\downarrow}\rangle$ have more weight in state $|\psi_a\rangle$ and $|\psi_b\rangle$ from Fig. 2.3 when $\widetilde{\beta}$ is small. Physically, it is because that the splitting energy levels start from $E_{1,\pm 3}^0$, and the effect coming from energy levels $E_{1,2,\downarrow}^0$, $E_{1,-2,\uparrow}^0$ can be seen as the correction of the energy. Therefore, we can distinguish which one of the elements of superposition states is domination in small $\widetilde{\beta}$.

Third, we deduce that the level repulsion is the reason of the two splitting energy levels arising up and going down respectively when $\widetilde{\beta}$ is small. Because of the first and second analysis, we know that the splitting energy level consists of the dominate energy level and the upper (lower) energy level. The upper or lower energy level play a repulsive role to effect the trend of the spectrum. For example, the original eigenstates in the eigenenergy $E_{1,\pm 3}^0$ split into two new degeneracy state $|\psi_a\rangle = c_1|E_{1,3,\uparrow}\rangle + c_2|E_{1,2,\uparrow}\rangle$ and $|\psi_b\rangle = c_3|E_{1,-2,\uparrow}\rangle + c_4|E_{1,-3,\downarrow}\rangle$. The lower energy $E_{1,\pm 2}^0$ repulses $E_{1,\pm 3}^0$ to arise up energy.

Fourth, in the next chapter, we will get the result about each of the perturbed states ($|\psi_a\rangle$, $|\psi_b\rangle$, $|\psi_c\rangle$ and $|\psi_d\rangle$) is not mixing by considering external magnetic flux. Therefore, we can use nondegenerate perturbation theory to analyze perturbation problems.

Fifth, in the small Dresselhaus strength region, we can get the trend of the energy level which is represented in the quadratic form. The reason can be demonstrated by two methods shown below. In nondegenerate perturbation theory, we can obtain the result,
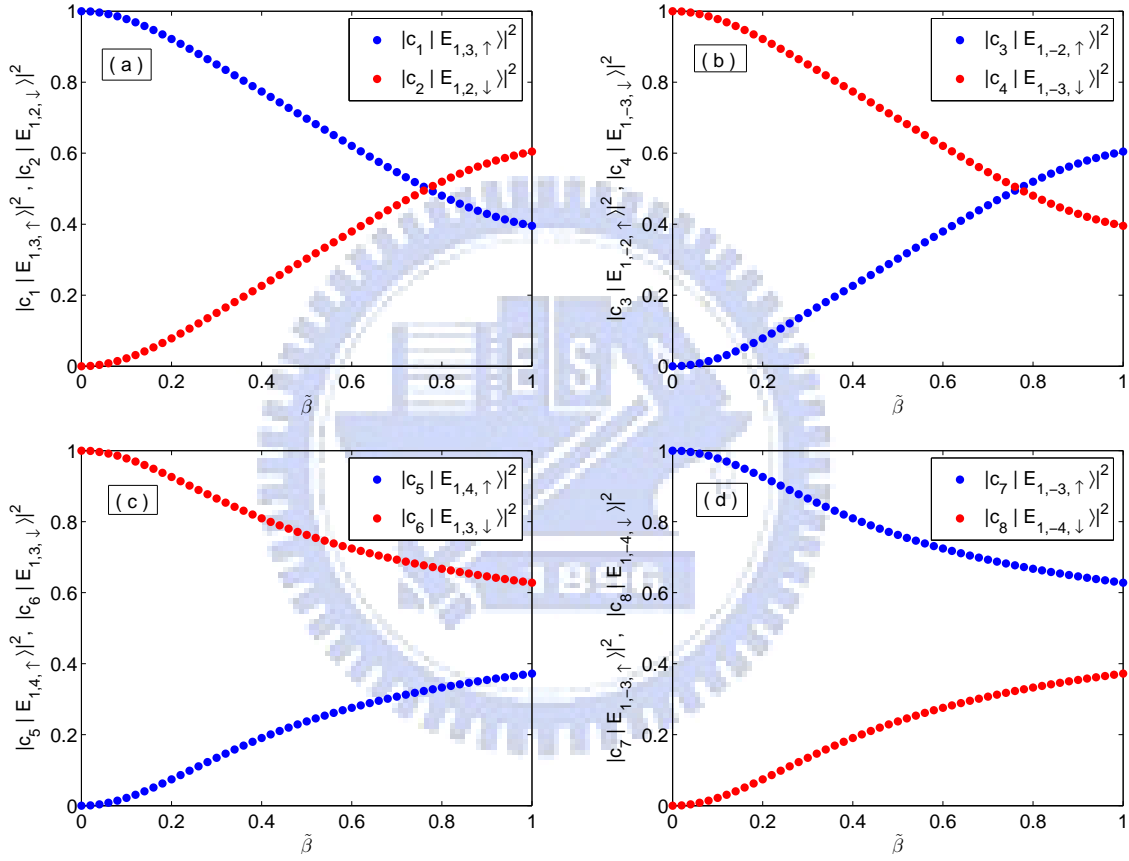
Figure 2.3: The relative weighting between the constituent bases state ket plays an important role to effect the trend of the energy spectrum. When the Dresselhaus strength is small: (a) $c_1 |E_{1,3,\uparrow}\rangle$ has more weight than $c_2 |E_{1,2,\uparrow}\rangle$ in state $|\psi_a\rangle$, (b) $c_4 |E_{1,-3,\downarrow}\rangle$ has more weight than $c_3 |E_{1,-2,\uparrow}\rangle$ in state $|\psi_b\rangle$, (c) $c_6 |E_{1,3,\downarrow}\rangle$ has more weight than $c_5 |E_{1,4,\uparrow}\rangle$ in state $|\psi_c\rangle$, (d) $c_7 |E_{1,-3,\uparrow}\rangle$ has more weight than $c_8 |E_{1,-4,\downarrow}\rangle$ in state $|\psi_d\rangle$.
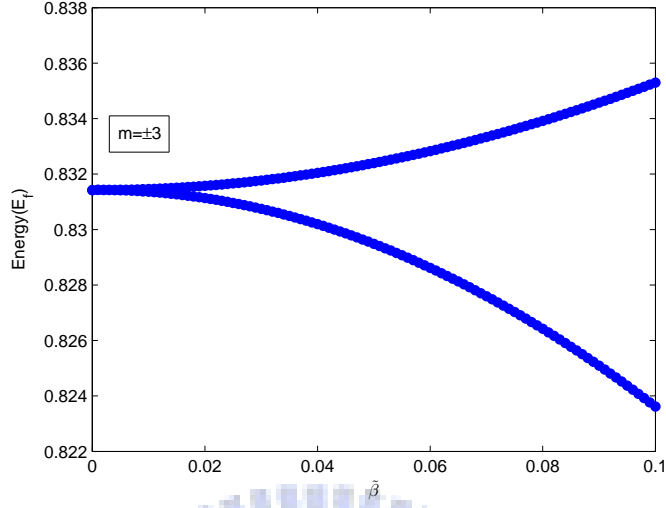
Figure 2.4: In the small Dresselhaus strength region, $0 \leq \widetilde{\beta} \leq 0.1$, we can get the trend of the energy level which is represented in the up (down) quadratic form. The physical parameters are the same with Fig. 2.2.

$$\langle n | H' | n \rangle + \sum_m \frac{\left| \langle m | H' | n \rangle \right|^2}{\varepsilon_n^0 - \varepsilon_m^0} \cong 0 + \sum_m \frac{\left| \langle m | H' | n \rangle \right|^2}{\varepsilon_n^0 - \varepsilon_m^0} \tag{2.25}$$

where the first order perturbation is equal to zero $\langle n | H' | n \rangle \cong 0$ and the second order perturbation is not. In other way, let us simplify the problem to a 2×2 matrix, then the Hamiltonian $H_0 + H_{DSO}$ can be represented as $\begin{pmatrix} \varepsilon_n & B \\ B & \varepsilon_m \end{pmatrix}$, where B is denoted as off-diagonal term proportional to DSO coupling strength. If we calculate the determination of this matrix when β is small, we can get the approximate eigenenergies.

$$\varepsilon = \frac{\varepsilon_n + \varepsilon_m}{2} \pm \frac{\varepsilon_n - \varepsilon_m}{2} \left(1 + \frac{1}{2} \left(\frac{2}{\varepsilon_n - \varepsilon_m} \right)^2 B^2 \right) \tag{2.26}$$

This result is the same as our numerical analysis which is shown in Fig. 2.4

Finally, we also find that there are two degeneracy eigenstates which are cause of the time-reversal symmetry in each new splitting energy level. If we use $-(m-1)$ to instead

of m in our Schrodinger equation Eq. (2.16), we can get the same couple Schrodinger equations which are meant to be Kramer degeneracy.

2.2.2 Spin density and net magnetic dipole moment

For a given eigenenergy $E_{n,m}$, a set coefficients of eigenfunction can be determined from the equation set Eq. (2.22). With the normalization condition $\int_{r_1}^{r_2} \psi_m^+ \psi_m \rho d\rho = 1$, we can obtain the uniquely determined eigenfunction Eq. (2.21).

If the general form of the eigenfunction is defined as $\psi_m (\widetilde{\rho}_r, \phi) = \begin{pmatrix} f_m (\widetilde{\rho}_r) e^{im\phi} \\ g_{m-1} (\widetilde{\rho}_r) e^{i(m-1)\phi} \end{pmatrix}$, the components of the spinor part eigenfunction are

$$f_m (\widetilde{\rho}_r) = aH_m^{(1)}(\gamma_1\widetilde{\rho}_r) + bH_m^{(2)}(\gamma_1\widetilde{\rho}_r) + cH_m^{(1)}(\gamma_2\widetilde{\rho}_r) + dH_m^{(2)}(\gamma_2\widetilde{\rho}_r) \tag{2.27}$$

$$g_{m-1} (\widetilde{\rho}_r) = i \left(-aH_{m-1}^{(1)}(\gamma_1\widetilde{\rho}_r) - bH_{m-1}^{(2)}(\gamma_1\widetilde{\rho}_r) + cH_{m-1}^{(1)}(\gamma_2\widetilde{\rho}_r) + dH_{m-1}^{(2)}(\gamma_2\widetilde{\rho}_r) \right) \tag{2.28}$$

Then, the particle density of each state m is $N_m (\widetilde{\rho}_r) = f_m^2 (\widetilde{\rho}_r) + g_{m-1}^2 (\widetilde{\rho}_r)$.

The spin density can be derived by the same method just like particle density. The z-projection spin density for each m state is $S_m^z (\widetilde{\rho}_r) = \psi_m^+ \sigma_z \psi_m = f_m^2 (\widetilde{\rho}_r) - g_{m-1}^2 (\widetilde{\rho}_r)$. By summing the contributions from ground state to the mth state, one can acquire the total spin density at zero temperature $S_z = \sum_m S_m^z (\widetilde{\rho}_r)$. The spin density as a function of dimensionless radial position $\widetilde{\rho}_r = \rho/r_1$ of the ring with each state is shown in Fig. 2.5 at DSO constant $\beta = 25 eV \cdot \overset{o}{A}$.

In Fig. 2.5, we can see that when we input single-electron in each state, the net z-projection spin is not zero, which can be seen as a magnetic dipole moment. But, because of the cancelation relation between states, there will left very few z-projection spins. Therefore, if we input odd-number of electrons in our system, we can get finite net total
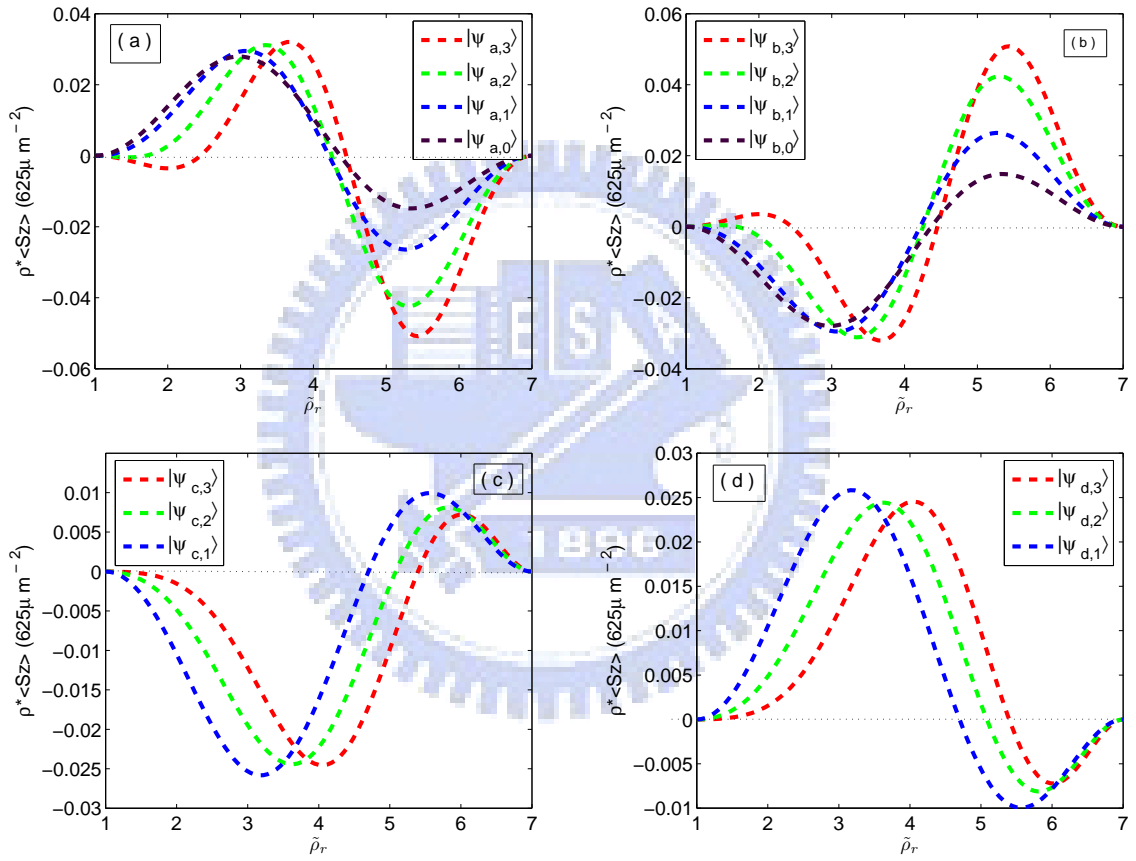
Figure 2.5: It is the z-projection spin density for each states as a function of the dimensionless radial length which the angular is fixed to zero.(a) $|\psi_{a,m}\rangle$ states, (b) $|\psi_{b,m}\rangle$ states, (c) $|\psi_{c,m}\rangle$ states, (d) $|\psi_{d,m}\rangle$ states.
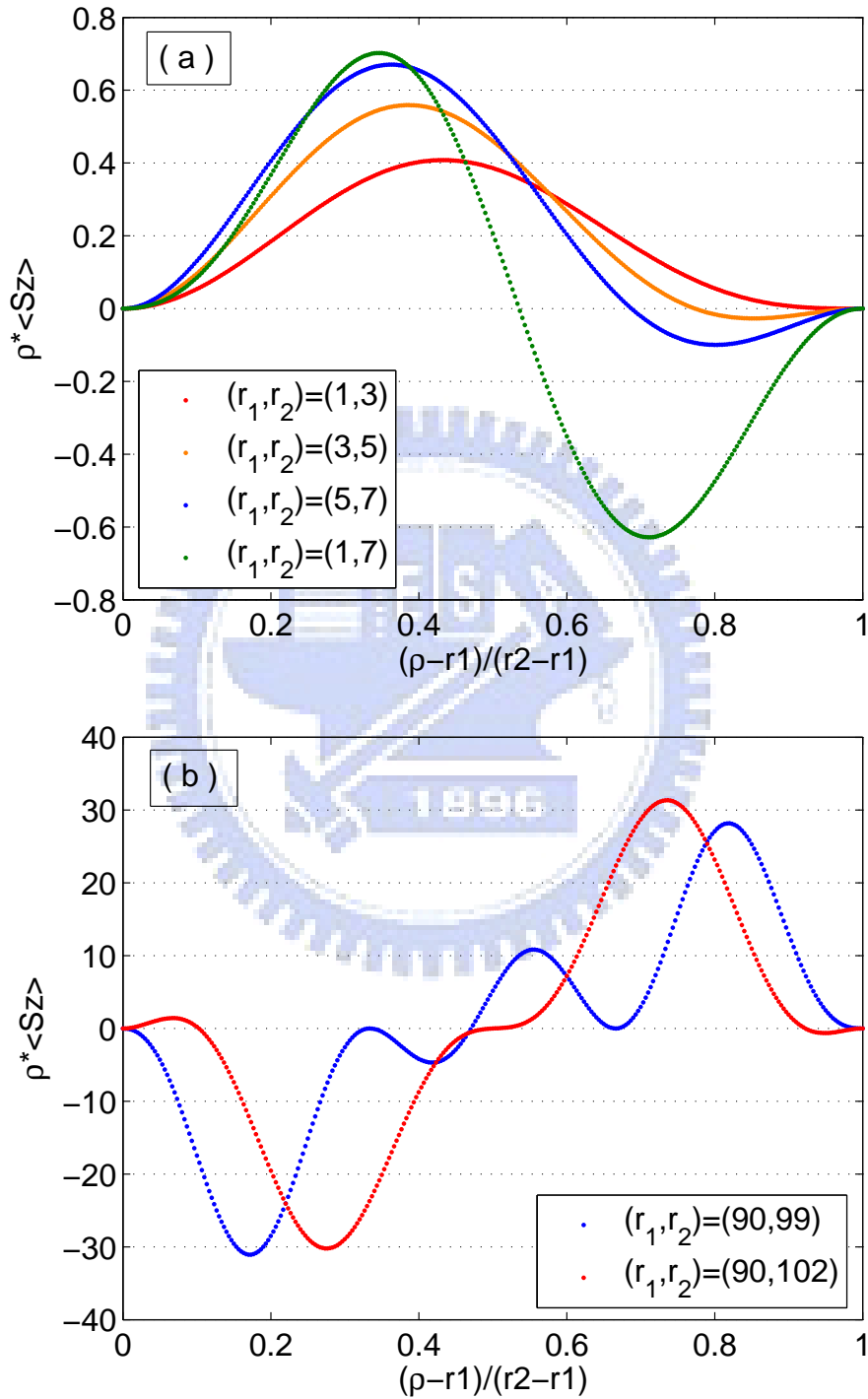
Figure 2.6: It is the z-projection spin density as a function of the radial ratio $\frac{\rho - r_1}{r_2 - r_1}$ which the angular is fixed to zero.(a) radial ratio in different range, (b) radial ratio is set as big as possible.

z-projection spin.

In the other way, we change the inner and outer radii for different range to observe the spin polarization phenomenon. Fig. 2.6 are the z-projection spin density as a function of radial ratio $\frac{\rho - r_1}{r_2 - r_1}$. We know that when the inner and outer radii become bigger in the same time, the ring width are more like a horizontal channel in the ring system. Therefore, we can see the effect of the different ring width between Fig. 2.6 (a) and Fig. 2.6 (b), then we make a simple conclusion: When the ring width is big enough, the spin accumulation phenomenon would be more observable.

Chapter 3

Finite width mesoscopic Dresselhaus spin-orbit (DSO) ring with a magnetic flux

3.1 Theoretical model

3.1.1 Hamiltonian

In this chapter, we start the system from the single-particle Hamiltonian which describes an electron in the mesoscopio ring piercing by a magnetic flux Φ with DSO coupling. The geometric model is almost the same with Fig. 2.1 in chapter 2. Therefore, we can write down the Hamiltonian quickly:

$$H \simeq \begin{pmatrix} \frac{p^2}{2m^*} + V & -\beta < k_z^2 > k_+ \\ -\beta < k_z^2 > k_- & \frac{p^2}{2m^*} + V \end{pmatrix}. \tag{3.1}$$

In order to consider adding the magnetic flux in our system, we should correct the momentum: (a) $p \rightarrow p - eA$; (b) $k \rightarrow k - \frac{eA}{\hbar}$, where A is the vector potential chosen as

the axial gauge. And the corresponding magnetic flux is $\frac{\Phi}{\Phi_0} = \frac{2\pi e A_\varphi \rho}{h} = \frac{e A_\varphi \rho}{\hbar}$ in units of flux quantum $\Phi_0 = \frac{h}{e}$.

In the following, just like in chapter 2, we guess the form of the eigenstate of H with the choice of quantum numbers parallel that of the unperturbed eigenstate $\left| E^0_{n,m,\sigma} \right\rangle$. Hints for the form of the eigenstate of H can be obtained from applying H_{DSO} repeatedly upon $\left| E^0_{n,m,\sigma} \right\rangle$. This amounts to give the form for the total eigenfunction where $f_1(\rho)$, $f_2(\rho)$ have to be solved explicitly.

$$\Psi = \begin{pmatrix} f_1(\rho) e^{im\varphi} \\ f_2(\rho) e^{i(m-1)\varphi} \end{pmatrix}. \tag{3.2}$$

By rewriting the Hamiltonian in polar coordinates and a hard-wall confinement potential defining the annulus is

$$V(\overrightarrow{\rho}, z) = \begin{cases} 0 & \text{for } r_1 < \rho < r_2 \text{ and } |z| < \frac{d}{2} \\ \infty & \text{otherwise} \end{cases} \tag{3.3}$$

we can get the coupling Schrodinger equations

$$\begin{cases} \frac{\hbar^2}{2m^*} \left[k^2 - 2 \left(\frac{\Phi}{\rho \Phi_0} \right) k_\varphi + \left(\frac{\Phi}{\rho \Phi_0} \right)^2 \right] f_1(\rho) e^{im\varphi} + i\beta \left(\frac{\pi}{d} \right)^2 e^{i\varphi} \left(\frac{\partial}{\partial \rho} + \frac{i}{\rho} \frac{\partial}{\partial \varphi} + \frac{\Phi}{\rho \Phi_0} \right) f_2(\rho) e^{i(m-1)\varphi} \\ = E f_1(\rho) e^{im\varphi} \\ \frac{\hbar^2}{2m^*} \left[k^2 - 2 \left(\frac{\Phi}{\rho \Phi_0} \right) k_\varphi + \left(\frac{\Phi}{\rho \Phi_0} \right)^2 \right] f_2(\rho) e^{i(m-1)\varphi} + i\beta \left(\frac{\pi}{d} \right)^2 e^{-i\varphi} \left(\frac{\partial}{\partial \rho} - \frac{i}{\rho} \frac{\partial}{\partial \varphi} - \frac{\Phi}{\rho \Phi_0} \right) f_1(\rho) e^{im\varphi} \\ = E f_2(\rho) e^{i(m-1)\varphi} \end{cases}$$

$$\tag{3.4}$$

3.1.2 Dimensionless

In order to get more clearly formula and prepare for the Numerical analysis, we set some parameters to dimensionless the Hamiltonian: (a) Fermi wave length l_f, (b) Fermi wave vector $k_f = \frac{1}{l_f}$, (c) Fermi energy $E_f = \frac{\hbar^2 k_f^2}{2m^*}$, (d) Del operator in polar coordinates $\nabla = k_f \widetilde{\nabla}$, (e) $p_{\rho,\varphi}^{\pm} = k_f \widetilde{p}_{\rho,\varphi}^{\pm}$, (f) $\widetilde{E} = \frac{E}{E_f}$, (g) $\widetilde{\beta} = \frac{\beta \left(\frac{\pi}{d}\right)^2 \cdot k_f}{E_f}$, (h) $\widetilde{\rho}_r = \frac{\rho}{r_1}$.

After calculation, we get the dimensionless couple equations (The detail process is shown in Appendix B.)

$$
\begin{cases}
\left\{ \frac{1}{\widetilde{\rho}} \frac{\partial}{\partial \widetilde{\rho}} \left(\widetilde{\rho} \frac{\partial}{\partial \widetilde{\rho}} \right) - \frac{1}{\widetilde{\rho}^2} \left(m - \frac{\Phi}{\Phi_0} \right)^2 \right\} f_1 \left(\widetilde{\rho}_r \right) e^{im\varphi} - i\widetilde{\beta} \left(\frac{\partial}{\partial \widetilde{\rho}} - \frac{1}{\widetilde{\rho}}(m - \frac{\Phi}{\Phi_0} - 1) \right) f_2 \left(\widetilde{\rho}_r \right) e^{im\varphi} \\
\quad = -\widetilde{E} f_1 (\widetilde{\rho}_r) e^{im\varphi} \\
\left\{ \frac{1}{\widetilde{\rho}} \frac{\partial}{\partial \widetilde{\rho}} \left(\widetilde{\rho} \frac{\partial}{\partial \widetilde{\rho}} \right) - \frac{1}{\widetilde{\rho}^2} \left(m - 1 - \frac{\Phi}{\Phi_0} \right)^2 \right\} f_2 \left(\widetilde{\rho}_r \right) e^{i(m-1)\varphi} - i\widetilde{\beta} \left(\frac{\partial}{\partial \widetilde{\rho}} + \frac{1}{\widetilde{\rho}} \left(m - \frac{\Phi}{\Phi_0} \right) \right) f_1 \left(\widetilde{\rho}_r \right) e^{i(m-1)\varphi} \\
\quad = -\widetilde{E} f_2 (\widetilde{\rho}_r) e^{i(m-1)\varphi}
\end{cases}
$$

$$(3.5)$$

Let $q = m - \frac{\Phi}{\Phi_0}$, Eq. (3.5) become

$$
\begin{cases}
\left\{ \frac{1}{\widetilde{\rho}} \frac{\partial}{\partial \widetilde{\rho}} \left(\widetilde{\rho} \frac{\partial}{\partial \widetilde{\rho}} \right) - \frac{q^2}{\widetilde{\rho}^2} \right\} f_1 \left(\widetilde{\rho}_r \right) e^{im\varphi} - i\widetilde{\beta} \left(\frac{\partial}{\partial \widetilde{\rho}} - \frac{1}{\widetilde{\rho}}(q - 1) \right) f_2 \left(\widetilde{\rho}_r \right) e^{im\varphi} = -\widetilde{E} f_1 (\widetilde{\rho}_r) e^{im\varphi} \\
\left\{ \frac{1}{\widetilde{\rho}} \frac{\partial}{\partial \widetilde{\rho}} \left(\widetilde{\rho} \frac{\partial}{\partial \widetilde{\rho}} \right) - \frac{(q-1)^2}{\widetilde{\rho}^2} \right\} f_2 \left(\widetilde{\rho}_r \right) e^{i(m-1)\varphi} - i\widetilde{\beta} \left(\frac{\partial}{\partial \widetilde{\rho}} + \frac{q}{\widetilde{\rho}} \right) f_1 \left(\widetilde{\rho}_r \right) e^{i(m-1)\varphi} = -\widetilde{E} f_2 (\widetilde{\rho}_r) e^{i(m-1)\varphi}
\end{cases}
$$

$$(3.6)$$

Since these differential equations have the forms of Bessel equation and the recurrence relation, we can choose the Bessel functions as the spinor part eigenfunctions. Therefore,

$$
\begin{cases}
-\gamma^2 A J_q(\gamma \widetilde{\rho}_r) - i\widetilde{\beta} \left[-\gamma B J_q(\gamma \widetilde{\rho}_r) \right] = -\widetilde{E} A J_q(\gamma \widetilde{\rho}_r) \\
-\gamma^2 B J_{q-1}(\gamma \widetilde{\rho}_r) - i\widetilde{\beta} \left[\gamma A J_{q-1}(\gamma \widetilde{\rho}_r) \right] = -\widetilde{E} B J_{q-1}(\gamma \widetilde{\rho}_r)
\end{cases}
$$

$$(3.7)$$

where A and B are the coefficients of the two eigenfunction components.

Comparing with above couple equations, we find that the ratio of the coefficients $R = \frac{B}{A} = \pm i$, then we get two branches of wave functions

$$\Psi = \begin{bmatrix} J_q(\gamma\widetilde{\rho}_r)e^{im\varphi} \\ iJ_{q-1}(\gamma\widetilde{\rho}_r)e^{i(m-1)\varphi} \end{bmatrix}, \Psi = \begin{bmatrix} J_q(\gamma\widetilde{\rho}_r)e^{im\varphi} \\ -iJ_{q-1}(\gamma\widetilde{\rho}_r)e^{i(m-1)\varphi} \end{bmatrix}. \tag{3.8}$$

3.1.3 Eigenenergy and Eigenstate

We get two energy dispersion $\gamma^2+\widetilde{\beta}\gamma-\widetilde{E} = 0$ and $\gamma^2-\widetilde{\beta}\gamma-\widetilde{E} = 0$ when R is equal to $+i$ and $-i$ respectively. Then, if we set $\gamma_1 = \frac{1}{2}\left(\widetilde{\beta} + \sqrt{\widetilde{\beta}^2 + 4\widetilde{E}}\right)$ and $\gamma_2 = \frac{1}{2}\left(-\widetilde{\beta} + \sqrt{\widetilde{\beta}^2 + 4\widetilde{E}}\right)$, we can obtain the total eigenfunction

$$\begin{aligned}\Psi = a\begin{pmatrix} H_q^{(1)}\left(\gamma_1\widetilde{\rho}_r\right)e^{im\varphi} \\ -iH_{q-1}^{(1)}\left(\gamma_1\widetilde{\rho}_r\right)e^{i(m-1)\varphi} \end{pmatrix} + b\begin{pmatrix} H_q^{(2)}\left(\gamma_1\widetilde{\rho}_r\right)e^{im\varphi} \\ -iH_{q-1}^{(2)}\left(\gamma_1\widetilde{\rho}_r\right)e^{i(m-1)\varphi} \end{pmatrix} \\ +c\begin{pmatrix} H_q^{(1)}\left(\gamma_2\widetilde{\rho}_r\right)e^{im\varphi} \\ iH_{q-1}^{(1)}\left(\gamma_2\widetilde{\rho}_r\right)e^{i(m-1)\varphi} \end{pmatrix} + d\begin{pmatrix} H_q^{(2)}\left(\gamma_2\widetilde{\rho}_r\right)e^{im\varphi} \\ iH_{q-1}^{(2)}\left(\gamma_2\widetilde{\rho}_r\right)e^{i(m-1)\varphi} \end{pmatrix} \end{aligned}, \tag{3.9}$$

where a, b, c and d are the coefficients.

Since the annulus is defined by the hard-wall confinement potential, we can apply the boundary conditions $\Psi\left(\rho = r_1\right) = 0$, $\Psi\left(\rho = r_2\right) = 0$. These conditions give the equation set:

$$\begin{pmatrix} H_q^{(1)}\left(\gamma_1 r_1\right) & H_q^{(2)}\left(\gamma_1 r_1\right) & H_q^{(1)}\left(\gamma_2 r_1\right) & H_q^{(2)}\left(\gamma_2 r_1\right) \\ -H_{q-1}^{(1)}\left(\gamma_1 r_1\right) & -H_{q-1}^{(2)}\left(\gamma_1 r_1\right) & H_{q-1}^{(1)}\left(\gamma_2 r_1\right) & H_{q-1}^{(2)}\left(\gamma_2 r_1\right) \\ H_q^{(1)}\left(\gamma_1 r_2\right) & H_q^{(2)}\left(\gamma_1 r_2\right) & H_q^{(1)}\left(\gamma_2 r_2\right) & H_q^{(2)}\left(\gamma_2 r_2\right) \\ -H_{q-1}^{(1)}\left(\gamma_1 r_2\right) & -H_{q-1}^{(2)}\left(\gamma_1 r_2\right) & H_{q-1}^{(1)}\left(\gamma_2 r_2\right) & H_{q-1}^{(2)}\left(\gamma_2 r_2\right) \end{pmatrix}\begin{pmatrix} a \\ b \\ c \\ d \end{pmatrix} = 0 \tag{3.10}$$

If there exists non-trivial solution for a, b, c and d, the determinant of the matrix M must vanish, i.e.,

$$\det\left(M\right) = 0, \tag{3.11}$$

where

$$
M = \begin{pmatrix}
H_q^{(1)}(\gamma_1 r_1) & H_q^{(2)}(\gamma_1 r_1) & H_q^{(1)}(\gamma_2 r_1) & H_q^{(2)}(\gamma_2 r_1) \\
-H_{q-1}^{(1)}(\gamma_1 r_1) & -H_{q-1}^{(2)}(\gamma_1 r_1) & H_{q-1}^{(1)}(\gamma_2 r_1) & H_{q-1}^{(2)}(\gamma_2 r_1) \\
H_q^{(1)}(\gamma_1 r_2) & H_q^{(2)}(\gamma_1 r_2) & H_q^{(1)}(\gamma_2 r_2) & H_q^{(2)}(\gamma_2 r_2) \\
-H_{q-1}^{(1)}(\gamma_1 r_2) & -H_{q-1}^{(2)}(\gamma_1 r_2) & H_{q-1}^{(1)}(\gamma_2 r_2) & H_{q-1}^{(2)}(\gamma_2 r_2)
\end{pmatrix}
\tag{3.12}
$$

The more detail process is shown in Appendix B.

3.2 Expression for charge current density

The Hamiltonian of the system including magnetic flux in polar coordinate is

$$
\begin{aligned}
H = &-\frac{\hbar^2}{2m^*}\left\{\frac{\partial^2}{\partial\rho^2} + \frac{1}{\rho}\frac{\partial}{\partial\rho} - \frac{1}{\rho^2}\left[-\frac{\partial^2}{\partial\varphi^2} + 2i\left(\frac{\Phi}{\Phi_0}\right)\frac{\partial}{\partial\varphi} + \left(\frac{\Phi}{\Phi_0}\right)^2\right]\right\} \\
&+i\beta\langle k_z^2\rangle\left[(e^{i\varphi}\sigma_+ + e^{-i\varphi}\sigma_-)\frac{\partial}{\partial\rho} + (e^{i\varphi}\sigma_+ - e^{-i\varphi}\sigma_-)\frac{1}{\rho}\left(i\frac{\partial}{\partial\varphi} + \frac{\Phi}{\Phi_0}\right)\right]
\end{aligned}
\tag{3.13}
$$

We start from time-dependent Schrodinger equation

$$
H\psi = i\hbar\frac{\partial\psi}{\partial t}.
\tag{3.14}
$$

Then, we put the complex conjugate wave function to operator Eq. (3.14):

$$
\begin{aligned}
\psi^+ i\hbar\frac{\partial\psi}{\partial t} = &-\frac{\hbar^2}{2m^*}\psi^+\left\{\frac{\partial^2}{\partial\rho^2} + \frac{1}{\rho}\frac{\partial}{\partial\rho} - \frac{1}{\rho^2}\left[-\frac{\partial^2}{\partial\varphi^2} + 2i\left(\frac{\Phi}{\Phi_0}\right)\frac{\partial}{\partial\varphi} + \left(\frac{\Phi}{\Phi_0}\right)^2\right]\right\}\psi \\
&+i\beta\langle k_z^2\rangle\psi^+\left[(e^{i\varphi}\sigma_+ + e^{-i\varphi}\sigma_-)\frac{\partial}{\partial\rho} + (e^{i\varphi}\sigma_+ - e^{-i\varphi}\sigma_-)\frac{1}{\rho}\left(i\frac{\partial}{\partial\varphi} + \frac{\Phi}{\Phi_0}\right)\right]\psi
\end{aligned}
\tag{3.15}
$$

At the same time, we change the wave function in Eq. (3.15) to become opposite complex conjugate form:

$$
\begin{aligned}
-\psi i\hbar\frac{\partial\psi^+}{\partial t} = &-\frac{\hbar^2}{2m^*}\psi\left\{\frac{\partial^2}{\partial\rho^2} + \frac{1}{\rho}\frac{\partial}{\partial\rho} - \frac{1}{\rho^2}\left[-\frac{\partial^2}{\partial\varphi^2} - 2i\left(\frac{\Phi}{\Phi_0}\right)\frac{\partial}{\partial\varphi} + \left(\frac{\Phi}{\Phi_0}\right)^2\right]\right\}\psi^+ \\
&-i\beta\langle k_z^2\rangle\psi\left[(e^{-i\varphi}\sigma_- + e^{i\varphi}\sigma_+)\frac{\partial}{\partial\rho} + (e^{-i\varphi}\sigma_- - e^{i\varphi}\sigma_+)\frac{1}{\rho}\left(-i\frac{\partial}{\partial\varphi} + \frac{\Phi}{\Phi_0}\right)\right]\psi^+
\end{aligned}
\tag{3.16}
$$

By combining Eq. (3.15) and Eq. (3.16), we can obtain the azimuthal component of the current density comparing with the continuity equation.

$$J_\varphi = \frac{-i\hbar}{2m^*\rho} \left[\psi^+ \frac{\partial \psi}{\partial \varphi} - \psi \frac{\partial \psi^+}{\partial \varphi} - 2i \left(\frac{\Phi}{\Phi_0} \right) \psi^+ \psi \right] - \frac{i}{\hbar} \beta \left\langle k_z^2 \right\rangle \left[e^{i\varphi} \psi^+ \sigma_+ \psi - e^{-i\varphi} \psi^+ \sigma_- \psi \right].$$

(3.17)

In other way, the general form of the wave function can be expressed briefly by defining its two components:

$$\Psi \equiv \begin{pmatrix} f_q(\widetilde{\rho}_r) e^{im\varphi} \\ g_{q-1}(\widetilde{\rho}_r) e^{i(m-1)\varphi} \end{pmatrix}$$

(3.18)

where

$$f_q(\widetilde{\rho}_r) = aH_q^{(1)}(\gamma_1 \widetilde{\rho}_r) + bH_q^{(2)}(\gamma_1 \widetilde{\rho}_r) + cH_q^{(1)}(\gamma_2 \widetilde{\rho}_r) + dH_q^{(2)}(\gamma_2 \widetilde{\rho}_r)$$

(3.19)

$$g_{q-1}(\widetilde{\rho}_r) = i \left[-aH_{q-1}^{(1)}(\gamma_1 \widetilde{\rho}_r) - bH_{q-1}^{(2)}(\gamma_1 \widetilde{\rho}_r) + cH_{q-1}^{(1)}(\gamma_2 \widetilde{\rho}_r) + dH_{q-1}^{(2)}(\gamma_2 \widetilde{\rho}_r) \right]$$

(3.20)

They give the terms in azimuthal component of current density :

$$\psi^+ \frac{\partial \psi}{\partial \varphi} - \psi \frac{\partial \psi^+}{\partial \varphi} = 2im f_q^* f_q + 2i(m-1) g_{q-1}^* g_{q-1}$$

(3.21)

$$\psi^+ \psi = f_q^* f_q + g_{q-1}^* g_{q-1}$$

(3.22)

$$\psi^+ \sigma_+ \psi = \begin{pmatrix} f_q^* e^{-im\varphi} & g_{q-1}^* e^{-i(m-1)\varphi} \end{pmatrix} \begin{pmatrix} 0 & 1 \\ 0 & 0 \end{pmatrix} \begin{pmatrix} f_q e^{im\varphi} \\ g_{q-1} e^{i(m-1)\varphi} \end{pmatrix} = f_q^* g_{q-1} e^{-i\varphi} \quad (3.23)$$

$$\psi^+ \sigma_- \psi = \begin{pmatrix} f_q^* e^{-im\varphi} & g_{q-1}^* e^{-i(m-1)\varphi} \end{pmatrix} \begin{pmatrix} 0 & 0 \\ 1 & 0 \end{pmatrix} \begin{pmatrix} f_q e^{im\varphi} \\ g_{q-1} e^{i(m-1)\varphi} \end{pmatrix} = g_{q-1}^* f_q e^{i\varphi} \quad (3.24)$$

If we set $\widetilde{v}_\beta = \frac{\beta \langle k_z^2 \rangle \cdot m^* r_1}{\hbar^2}$, we can get the azimuthal component of the current density:

$$J_\varphi = \frac{\hbar}{m^* r_1} \left\{ \frac{1}{\widetilde{\rho}} \left[q f_q^* f_q + (q-1) g_{q-1}^* g_{q-1} \right] - i \widetilde{v}_\beta \left[f_q^* g_{q-1} - g_{q-1}^* f_q \right] \right\} \qquad (3.25)$$

The total charge current density at zero temperature is the sum of the contribution from ground state to the Nth state where N is the total electron number. In the absence of magnetic flux, the distribution of the total charge current density is zero even in the presence of DSO coupling.

3.3 Numerical results and discussion

3.3.1 Energy spectrum - Removal of degeneracy

Physical parameters used in the below calculation are obtained for the case of GaAs: with DSO coupling constant $\beta = 25eV \cdot \overset{o}{A}$, effective mass $m^* \approx 0.067 m_e$. Structures parameters are inner radius $r_1 = 10nm$ and outer radius $r_2 = 70nm$. The energy spectrum which is plotted in the range of $-0.6 < \frac{\Phi}{\Phi_0} < 0.6$ adopted the same parameters in chapter 2 before.

Fig. 3.1 is the energy spectrum displayed as a function of the magnetic flux $\frac{\Phi}{\Phi_0}$ in our system which is obtained from the determinant equation $\det (M) = 0$, and $\tilde{\beta}$ is turned off in (a) turned on in (b). The dimensionless energy E is eigenenergy in units of $E_f = \frac{\hbar^2 k_f^2}{2m}$. In Fig. 3.1 (b), we see that each of the discrete eigenenergy splits into two parts (arising up and going down) when we turn on external magnetic flux, and it is interesting that the bigger m become, the wider energy splitting would be.

In order to observe the development of the energy levels and eigenstates easily, we combined Fig. 2.2 and Fig. 3.1 (b) artificial. In x-axis, left hand side is the dimensionless DSO coupling strength $\tilde{\beta}$ from 0 to 1, and right hand side is magnetic flux Φ/Φ_0 from 0 to 0.6 (keep $\tilde{\beta} = 1$). Then, we will discuss some issue about the eigenstates and the effect of the external magnetic flux in this section.
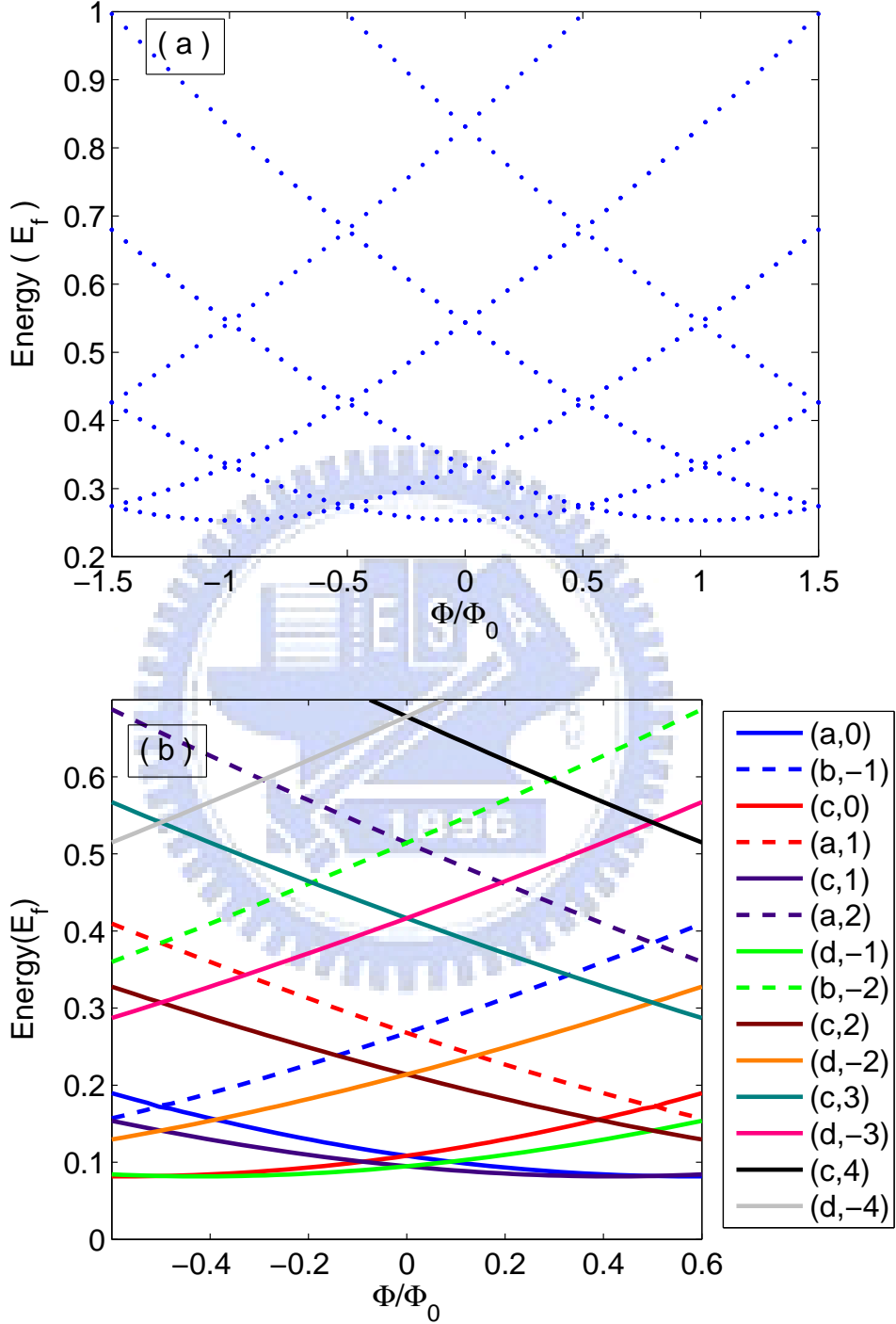
Figure 3.1: (a) Several lowest dimensionless eigenenergies E as a function of the magnetic flux Φ/Φ_0 for the quantum ring without DSOI, (b) with DSO coupling constant $\beta = 25eV \cdot \overset{o}{A}$. Where the legend denotes the state in the form of (η , m), η is a, b, c or d and m is the dominated magnetic quantum number. The other physical parameters are obtained for the case of GaAs: $m^* \approx 0.067m_e$, $\lambda_f = 40nm$, $r_1 = 10nm$, $r_2 = 70nm$, $d = 50 \overset{o}{A}$.
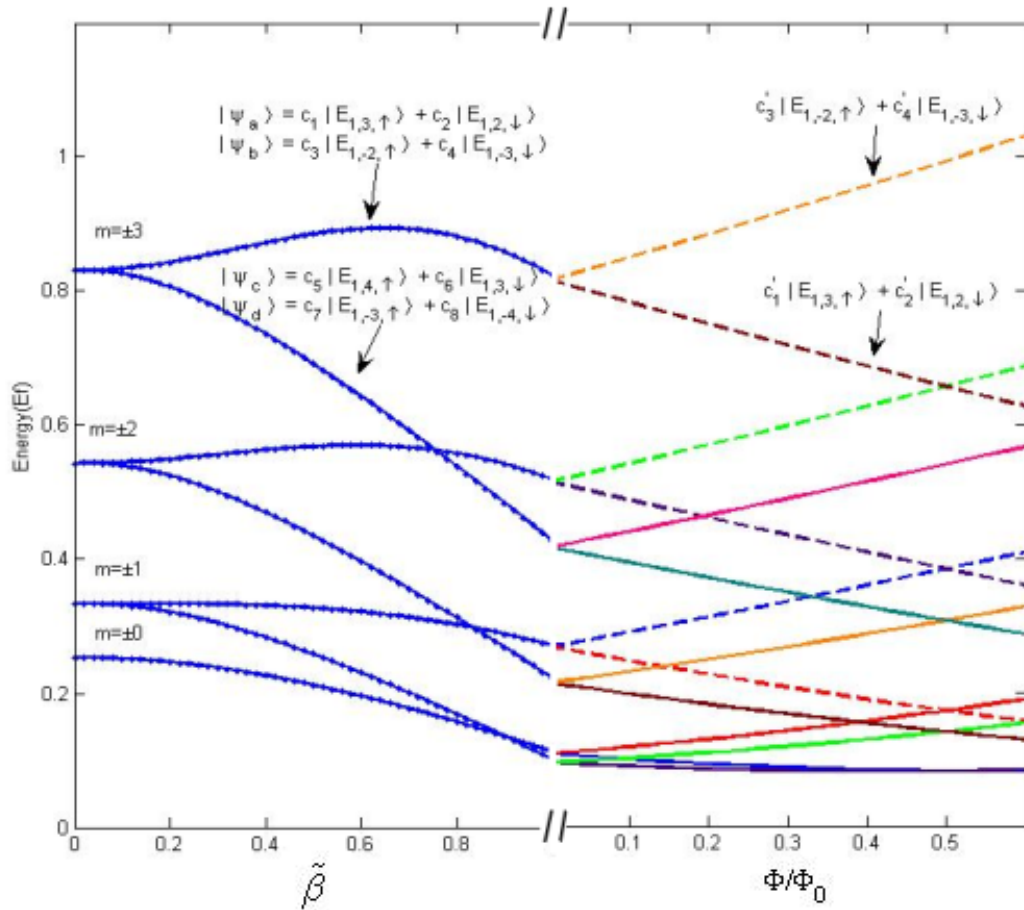
Figure 3.2: Left hand side is the the several lowest dimensionless eigenenergies E as a function of the dimensionless DSO coupling strength $\tilde{\beta}$ from 0 to 1, right hand side is the eigenenergies as a function of the magnetic flux Φ/Φ_0 from 0 to 0.6. The physical parameters are the same with Fig. 3.1.

First, we found a simple rule for the removal of the degeneracy when Φ is turned on. This analysis should be demonstrated by the operator form:

$$H_\Phi = \left(\frac{1}{\rho}\frac{\Phi}{\Phi_0}\right)\left[i\left(e^{-i\varphi}k_+ - e^{i\varphi}k_-\right) + \left(\frac{1}{\rho}\frac{\Phi}{\Phi_0}\right) + i\beta\left(e^{i\varphi}\sigma_+ - e^{-i\varphi}\sigma_-\right)\right]. \tag{3.26}$$

In Eq. (3.26), we find that there are no correction about the orbit-angular moment and spin-angular moment in the first several terms, but yes in the last two terms. For example, there are two degeneracy states $|\psi_a\rangle = c_1|E_{1,3,\uparrow}\rangle + c_2|E_{1,2,\downarrow}\rangle$ and $|\psi_b\rangle = c_3|E_{1,-2,\uparrow}\rangle + c_4|E_{1,-3,\downarrow}\rangle$ in the same eigenenergy. If we add, however, the magnetic flux to our system, we find that original degeneracy energy level split into two new energy levels, $c_3'|E_{1,-2,\uparrow}\rangle + c_4'|E_{1,-3,\downarrow}\rangle$ and $c_1'|E_{1,3,\uparrow}\rangle + c_2'|E_{1,2,\downarrow}\rangle$. The analysis is the same as the H_{DSO} repeatedly operating on original states in section 2.2.1. Therefore, H_Φ can not create new states by magnetic flux but just recombined original states.

Second, the external magnetic flux will split energy level again without mixing. Assuming $m' > 0$, then we can redefine $|\psi_a\rangle = c_1|E_{n,m',\uparrow}\rangle + c_2|E_{n,m'-1,\downarrow}\rangle$ and $|\psi_b\rangle = c_3|E_{n,-(m'-1),\uparrow}\rangle + c_4|E_{n,-m',\downarrow}\rangle$. After considering magnetic flux, the effective correctional Hamiltonian in matrix form is

$$H_\Phi = \left(\frac{1}{\rho}\frac{\Phi}{\Phi_0}\right)\begin{pmatrix} \frac{2i}{\rho}\frac{\partial}{\partial\varphi} + \frac{1}{\rho}\frac{\Phi}{\Phi_0} & i\beta e^{i\varphi} \\ -i\beta e^{-i\varphi} & \frac{2i}{\rho}\frac{\partial}{\partial\varphi} + \frac{1}{\rho}\frac{\Phi}{\Phi_0} \end{pmatrix}. \tag{3.27}$$

Then, we calculate the expectative value $\langle\psi_a|H_\Phi|\psi_b\rangle$ which is equal to zero and understand that the original degeneracy states which exist in $H_0 + H_{DSO}$ just split again without mixing respectively after considering external magnetic flux (The detail is shown in appendix. C).

Third, we demonstrated that states with $m_z < 0$ have higher energy than states with $m_z > 0$. If Φ is small, H_Φ can be redefine as first order perturbation:

$$H_{\Phi}^{(1)} = \left(\frac{1}{\rho}\frac{\Phi}{\Phi_0}\right)\begin{pmatrix} \frac{2i}{\rho}\frac{\partial}{\partial\varphi} & i\beta e^{i\varphi} \\ -i\beta e^{-i\varphi} & \frac{2i}{\rho}\frac{\partial}{\partial\varphi} \end{pmatrix}. \tag{3.28}$$

Then, we get the expectative value of $H_{\Phi}^{(1)}$ by using state $|\psi_a\rangle$ and state $|\psi_b\rangle$ respectively. (The detail is shown in appendix. D)

$$\langle\psi_a|\,H_{\Phi}^{(1)}\,|\psi_a\rangle = \langle\psi_b|\,H_{\Phi}^{(1)}\,|\psi_b\rangle = -\left(\frac{\Phi}{\Phi_0}\right)\int\left\{\frac{1}{\rho^2}\left[(2m-1)\,N_m + S_z\right] + \left(\frac{1}{\rho}\right)\beta S_{y(\varphi=0)}\right\}dv, \tag{3.29}$$

where $N_m = \psi^+\psi = f_q^* f_q + g_{q-1}^* g_{q-1}$, $S_z = \psi^+\sigma_z\psi = f_q^* f_q - g_{q-1}^* g_{q-1}$, and $S_y = i\left[-f_{n,m}^*(\rho)\,g_{n,m-1}(\rho)\,e^{-i\varphi} + g_{n,m-1}^*(\rho)\,f_{n,m}(\rho)\,e^{i\varphi}\right]$. It is reasonable for us to understand that when $m > 0$, the correction of the energy goes down, when $m < 0$, the correction of the energy goes up. The trend is shown in Fig. 3.2.

Finally, we also got a reasonable explanation for the phenomenon that the higher the state becomes, the wider energy splitting would be. Base on the third discussion, we can tell that the scaler of the energy splitting is proportional to $\langle\psi_b|\,H_{\Phi}^{(1)}\,|\psi_b\rangle - \langle\psi_a|\,H_{\Phi}^{(1)}\,|\psi_a\rangle \propto 2\,(2m-1)\left(\frac{\Phi}{\Phi_0}\right)\int\frac{N_m}{\rho^2}dv$. Thus, the energy splitting range is dependent of m, in other words, the bigger m becomes, the wider energy splitting would be.

3.3.2 Persistent charge current

The total persistent charge current at zero temperature can be obtained from the charge current density of each state through summing the contributions from all occupied states, i.e., $I = \int_{r_1}^{r_2}\left[\sum_m J_m\right]d\rho = -\frac{\partial E}{\partial\Phi}$. The total persistent charge current and the angular momentum Sz, Lz, $Sz + Lz$, $Lz(\tilde{\beta} = 0.01)$ with even number electrons $N = 8$ as a function of magnetic flux $\frac{\Phi}{\Phi_0}$ are shown in the Fig. 3.3 and Fig. 3.4.
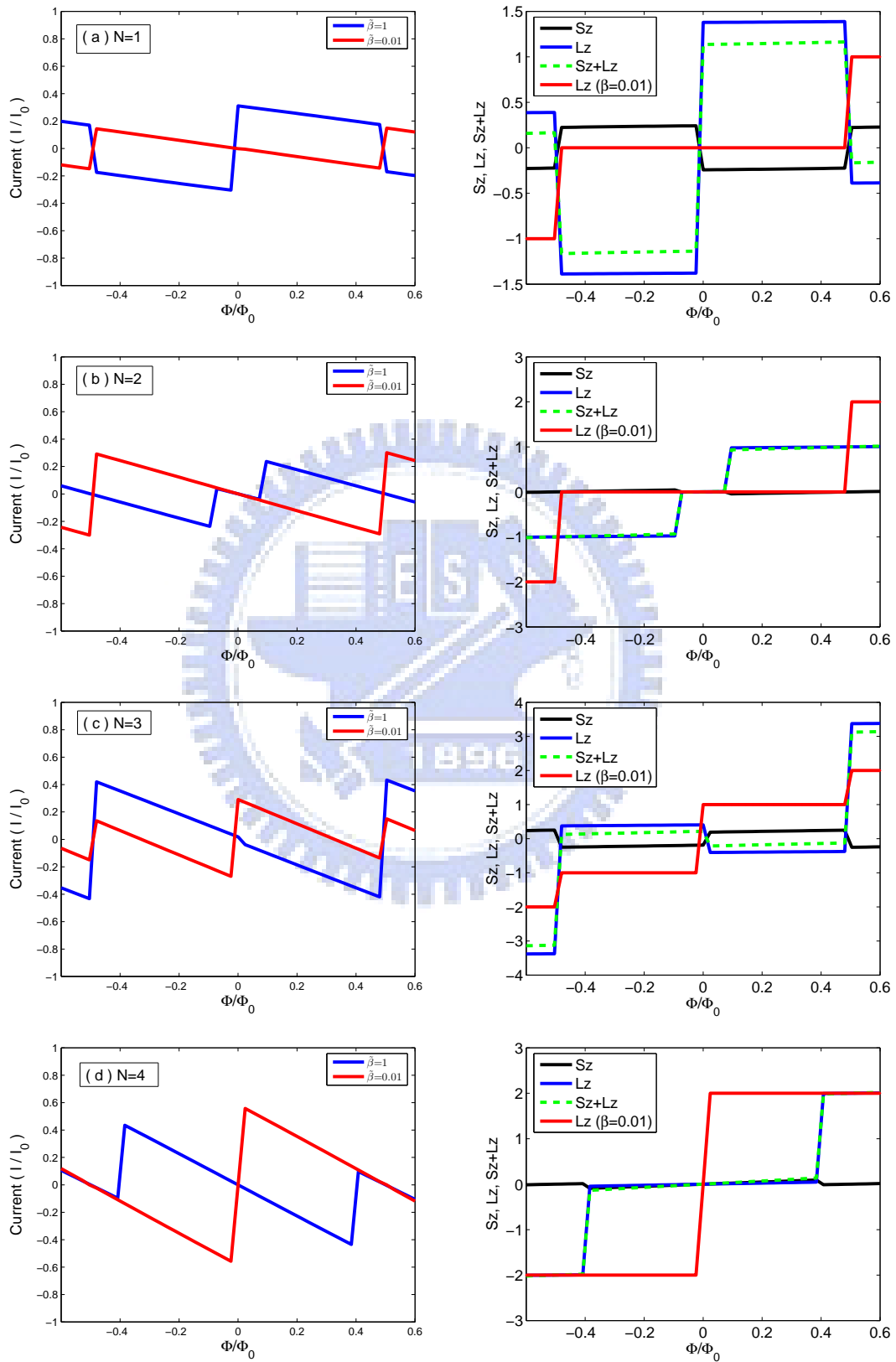
Figure 3.3: Electron numbers from $N = 1$ to $N = 4$, left hand side is the total persistent charge current of the quantum ring as a function of magnetic flux Φ/Φ_0, right hand side is Sz, Lz, $Sz + Lz$ and $Lz(\tilde{\beta} = 0.01)$ as a function of magnetic flux Φ/Φ_0.
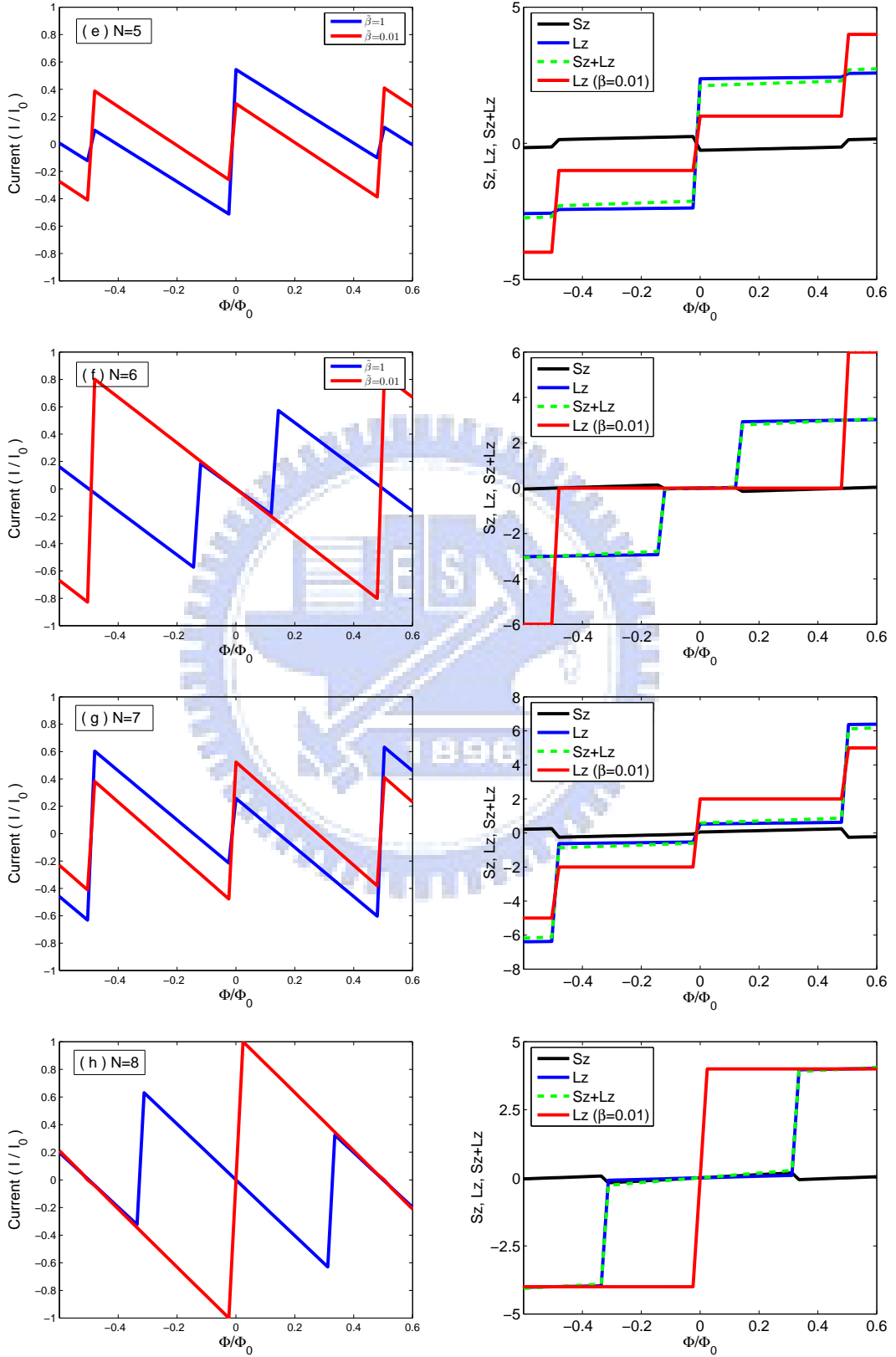
Figure 3.4: Electron numbers from $N = 5$ to $N = 8$, left hand side is the total persistent charge current of the quantum ring as a function of magnetic flux Φ/Φ_0, right hand side is Sz, Lz, $Sz + Lz$ and $Lz(\tilde{\beta} = 0.01)$ as a function of magnetic flux Φ/Φ_0.

It is well-known that the persistent charge current has a universal behavior independent of N when N is large enough. But, when N is small, the total number of electrons is important. Base on above reasons, we are careful about details in Fig. 3.3 and Fig. 3.4. We found that the characteristic features of persistent charge current depends on the parity of the total number of electrons N. At the point of the magnetic flux $\Phi = 0$, there is an abrupt jump when N is odd and continuous when N is even. Therefore, these characteristic features can be distinguished by two groups with N odd and N even. This is attributed to the different occupation patterns of the highest occupied single particle energy level. The same with the persistent current, the total z-projection magnetic moment including spin S_z and angular moment L_z have similar features, too. Near the magnetic flux $\Phi = 0$, there is an abrupt jump when N is odd and flat when N is even. These results can be a hint for us to distinguish the electron numbers which are even or odd. And it is a useful method to double check the experimental results by electrical and magnetic measurements.
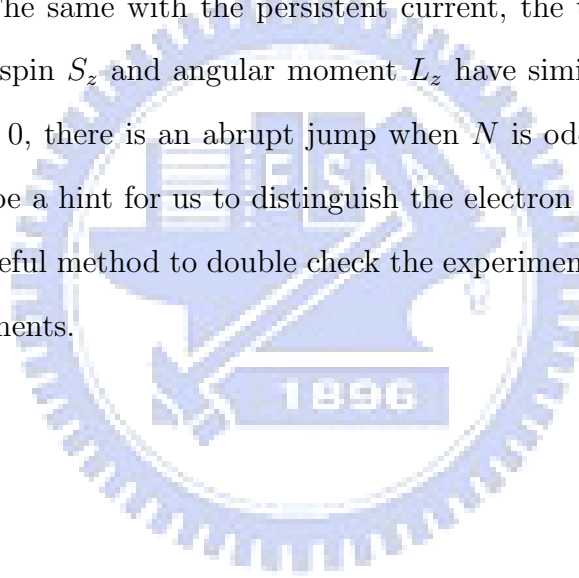
Chapter 4

Conclusion and future work

4.1 Conclusion

In Chapter1, we survey some journal papers to understand the background of the spin-orbital interaction (SOI) and the persistent current. According to the physical origin of the SOI, the SOI can be divided into intrinsic and extrinsic types, the extrinsic type SOI comes from the effective field of the impurity and the intrinsic type SOI comes from the structural effect. In intrinsic regime, the SOI in semiconductors requires an effective electric field in the material. Such effective electric field can find contribution from the build-in crystal field when the crystal has bulk inversion asymmetric (BIA) the so-called Dresselhaus SOI, or structural inversion asymmetry (SIA), the so-called Rashba SOI.

In other way, the persistent current can be trace from the AB effect, and the first one who proposed a model in a one-dimensional mental ring threaded by a flux to discuss band structure was Buttiker et al. in 1983. Until now, the persistent current is still an interesting issue for scientists to focus on, like Splettstosser et al., they proposed a mesoscopic isolated quasi-one-dimension ring with Rashba SOI threaded by magnetic flux at low temperature. They found some regulations about the persistent current and persistent spin current.

In Chapter2, we propose a geometric model which is an isolated finite width mesoscopic

ring with Dresselhaus spin-orbit (DSO) coupling without any external electromagnetic field to discuss eigenstates, energy spectrum and spin density. Moreover, we make some limiting case and perturbation to discuss the physical insight between the eigenstates, energy levels, and spin density. In our case, if we just consider the effect of the confinement potential in the quantum ring, we can get the discrete quantum energy levels and each of them has different degeneracy states respectively. But, if we add the DSO interaction to our system, we find that each unperturbed degeneracy energy level split into two groups of energy levels, and the new one exists new degeneracy states which is the superposition of the unperturbed eigenstates in H_0.

After some detail analysis, we propose a systematic method to understand the development of the states, and the trend of the energy spectrum is understood by level repulsions and the relative weighting between the constituent bases state ket. The energy spectrum depends on the DSOI quadratically in the weak SOI field regime, which is consistent with our perturbation result. Finally, we demonstrate that all energy levels are doubly degenerate, of the Kramer's type. In other way, we obtain same results about the z-projection spin density. When we input single-electron in each state, the net z-projection spin is not zero, which can be seen as a magnetic dipole moment. But, because of the cancelation relation between states, there will left finite z-projection spins.

In Chapter3, we start our research from the same system as chapter 2 but threaded by an external magnetic flux Φ to discuss the physical insight of the eigenstates and energy levels. After many analysis, we find a simple way using H_Φ to understand the perturbed statesas as the same meyhod as H_{DSO} shown in chapter 2, and demonstrate that the energy level will split into higher and lower energy levels after considering magnetic flux. Besides, we also got a reasonable explanation for the phenomenon that the higher the state becomes, the wider energy splitting would be. The most important is that we show the Kramer degenerate states splitting and the physical reason for the subsequent order in the energy splitting is identified.

4.2 Future works

Although we spend much time focusing on the physical insight about the eigenstates and energy spectrum in DSOI mesoscopic ring, there are still some problems need us to solve. First, we still don't know which is the domination between level repulsion effect and the relative weighting in the constituent bases state ket when DSOI strength is increasing. Second, the spin hall effect may be seen in finite width mesoscopic ring when the width is big enough. Third, there should be some relationships between the persistent currents and angular moment when we input different number electrons, furthermore, we can propose an experimental model to check it's realistic in the future.

In the future, we will study those topics which we have not finished, and try to solve our problem in different method like using tight-binding model.
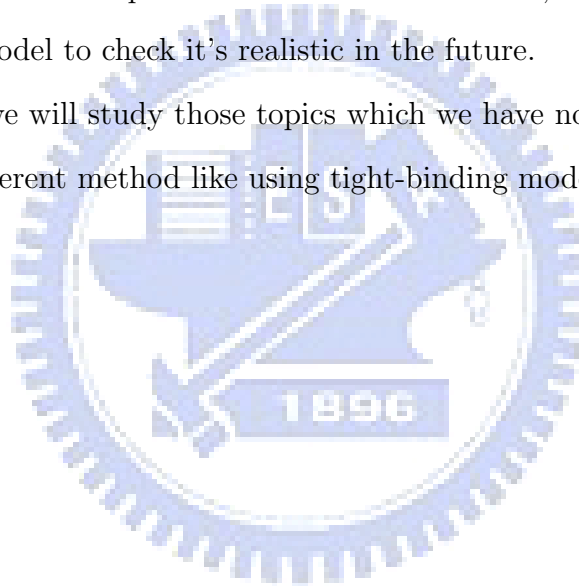
Appendix A

Solve the finite width mesoscopic ring Hamiltonian with DSO coupling

The finite width mesoscopic ring Hamiltonian with DSO coupling:

$$
H \cong \begin{pmatrix} \frac{p^2}{2m^*} + V & -\beta < k_z^2 > k_+ \\ -\beta < k_z^2 > k_- & \frac{p^2}{2m^*} + V \end{pmatrix} = \begin{pmatrix} \frac{p^2}{2m^*} + V & i\beta(\frac{\pi}{d})^2 e^{i\varphi} p_{\rho,\varphi}^+ \\ i\beta(\frac{\pi}{d})^2 e^{-i\varphi} p_{\rho,\varphi}^- & \frac{p^2}{2m^*} + V \end{pmatrix}. \quad \text{(A.1)}
$$

Because of the analysis in chapter 2, we guess the form of the total eigenfunction is

$$
\Psi = \begin{pmatrix} f_1(\rho) e^{im\varphi} \\ f_2(\rho) e^{i(m-1)\varphi} \end{pmatrix}, \quad \text{(A.2)}
$$

where $f_1(\rho)$ and $f_2(\rho)$ have to be solved explicitly.

For a hard-wall confinement potential

$$
V(\overrightarrow{\rho}, z) = \begin{cases} 0 & \text{for } r_1 < \rho < r_2 \text{ and } |z| < \frac{d}{2} \\ \infty & \text{otherwise} \end{cases} \quad \text{(A.3)}
$$

the Schrodinger equations inside the ring is given by

$$
\begin{pmatrix}
\frac{p^2}{2m^*} & i\beta(\frac{\pi}{d})^2 e^{i\varphi} p_{\rho,\varphi}^+ \\
i\beta(\frac{\pi}{d})^2 e^{-i\varphi} p_{\rho,\varphi}^- & \frac{p^2}{2m^*}
\end{pmatrix}
\begin{pmatrix}
f_1(\rho)e^{im\varphi} \\
f_2(\rho)e^{i(m-1)\varphi}
\end{pmatrix}
= E
\begin{pmatrix}
f_1(\rho)e^{im\varphi} \\
f_2(\rho)e^{i(m-1)\varphi}
\end{pmatrix}. \quad (A.4)
$$

In order to get more clearly formula and prepare for the Numerical analysis, we set some parameters to dimensionless the Hamiltonian: (a) Fermi wave length l_f, (b) Fermi wave vector $k_f = \frac{1}{l_f}$, (c) Fermi energy $E_f = \frac{\hbar^2 k_f^2}{2m^*}$, (d) Del operator in polar coordinates $\nabla = k_f \widetilde{\nabla}$, (e) $p_{\rho,\varphi}^\pm = k_f \widetilde{p}_{\rho,\varphi}^\pm$, (f) $\widetilde{E} = \frac{E}{E_f}$, (g) $\widetilde{\beta} = \frac{\beta\left(\frac{\pi}{d}\right)^2 \cdot k_f}{E_f}$, (h) $\widetilde{\rho}_r = \frac{\rho}{r_1}$.

$$
\begin{cases}
-\frac{\hbar^2 k_f^2}{2m^*} \widetilde{\nabla}^2 \left[f_1(\widetilde{\rho}_r)e^{im\varphi}\right] + i\beta(\frac{\pi}{d})^2 e^{i\varphi} k_f \widetilde{p}_{\rho,\varphi}^+ \left[f_2(\widetilde{\rho}_r)e^{i(m-1)\varphi}\right] = E f_1(\widetilde{\rho}_r)e^{im\varphi} \\
-\frac{\hbar^2 k_f^2}{2m^*} \widetilde{\nabla}^2 \left[f_2(\widetilde{\rho}_r)e^{i(m-1)\varphi}\right] + i\beta(\frac{\pi}{d})^2 e^{-i\varphi} k_f \widetilde{p}_{\rho,\varphi}^- \left[f_1(\widetilde{\rho}_r)e^{im\varphi}\right] = E f_2(\widetilde{\rho}_r)e^{i(m-1)\varphi}
\end{cases} \quad (A.5)
$$

$$
\begin{cases}
-\widetilde{\nabla}^2 \left[f_1(\widetilde{\rho}_r)e^{im\varphi}\right] + i\widetilde{\beta} e^{i\varphi} \left[\frac{\partial}{\partial\widetilde{\rho}} + i\frac{1}{\widetilde{\rho}}\frac{\partial}{\partial\varphi}\right] \left[f_2(\widetilde{\rho}_r)e^{i(m-1)\varphi}\right] = \widetilde{E} f_1(\widetilde{\rho}_r)e^{im\varphi} \\
-\widetilde{\nabla}^2 \left[f_2(\widetilde{\rho}_r)e^{i(m-1)\varphi}\right] + i\widetilde{\beta} e^{-i\varphi} \left[\frac{\partial}{\partial\widetilde{\rho}} - i\frac{1}{\widetilde{\rho}}\frac{\partial}{\partial\varphi}\right] \left[f_1(\widetilde{\rho}_r)e^{im\varphi}\right] = \widetilde{E} f_2(\widetilde{\rho}_r)e^{i(m-1)\varphi}
\end{cases} \quad (A.6)
$$

$$
\begin{cases}
\widetilde{\nabla}^2 \left[f_1(\widetilde{\rho}_r)e^{im\varphi}\right] - i\widetilde{\beta} e^{im\varphi} \left[\frac{\partial}{\partial\widetilde{\rho}} f_2(\widetilde{\rho}_r) - \frac{(m-1)}{\widetilde{\rho}} f_2(\widetilde{\rho}_r)\right] = -\widetilde{E} f_1(\widetilde{\rho}_r)e^{im\varphi} \\
\widetilde{\nabla}^2 \left[f_2(\widetilde{\rho}_r)e^{i(m-1)\varphi}\right] - i\widetilde{\beta} e^{i(m-1)\varphi} \left[\frac{\partial}{\partial\widetilde{\rho}} f_1(\widetilde{\rho}_r) + \frac{m}{\widetilde{\rho}} f_1(\widetilde{\rho}_r)\right] = -\widetilde{E} f_2(\widetilde{\rho}_r)e^{i(m-1)\varphi}
\end{cases} \quad (A.7)
$$

We compare the second term of above equations with the properties of Bessel function:(a) $\frac{\partial}{\partial\rho} J_{m-1} - \frac{m-1}{\rho} J_{m-1} = -\gamma J_m$, (b) $\frac{\partial}{\partial\rho} J_m + \frac{m}{\rho} J_m = \gamma J_{m-1}$, (c) $\left[\frac{1}{\rho}\frac{\partial}{\partial\rho}(\rho\frac{\partial}{\partial\rho}) - \frac{m^2}{\rho^2}\right] J_m(\gamma\rho) = -\gamma^2 J_m(\gamma\rho)$, therefore,

$$
\begin{cases}
-\gamma^2 A J_m(\gamma\widetilde{\rho}_r)e^{im\varphi} - i\widetilde{\beta}\left[-\gamma B J_m(\gamma\widetilde{\rho}_r)\right] e^{im\varphi} = -\widetilde{E} A J_m(\gamma\widetilde{\rho}_r)e^{im\varphi} \\
-\gamma^2 B J_{m-1}(\gamma\widetilde{\rho}_r)e^{i(m-1)\varphi} - i\widetilde{\beta}\left[\gamma A J_{m-1}(\gamma\widetilde{\rho}_r)\right] e^{i(m-1)\varphi} = -\widetilde{E} B J_{m-1}(\gamma\widetilde{\rho}_r)e^{i(m-1)\varphi}
\end{cases} \quad (A.8)
$$

$$\begin{cases} \gamma^2 A - i\widetilde{\beta}\gamma B = \widetilde{E}A \\ \gamma^2 B + i\widetilde{\beta}\gamma A = \widetilde{E}B \end{cases} \tag{A.9}$$

let $R = \frac{B}{A}$ as the ratio of the coefficient A,B

$$\begin{cases} \gamma^2 - i\widetilde{\beta}\gamma R = \widetilde{E} \\ \gamma^2 + i\widetilde{\beta}\gamma R^{-1} = \widetilde{E} \end{cases} \tag{A.10}$$

Comparing above equations, we get the ratio $R = \pm i$, but there are two branches of wave functions. When $R = +i$, wave function is

$$\Psi = \begin{bmatrix} J_m(\gamma\widetilde{\rho}_r)e^{im\varphi} \\ iJ_{m-1}(\gamma\widetilde{\rho}_r)e^{i(m-1)\varphi} \end{bmatrix}, \tag{A.11}$$

when $R = -i$, wave function is

$$\Psi = \begin{bmatrix} J_m(\gamma\widetilde{\rho}_r)e^{im\varphi} \\ -iJ_{m-1}(\gamma\widetilde{\rho}_r)e^{i(m-1)\varphi} \end{bmatrix}. \tag{A.12}$$

After setting $\gamma_1 = \frac{1}{2}\left(\widetilde{\beta} + \sqrt{\widetilde{\beta}^2 + 4\widetilde{E}}\right)$ and $\gamma_2 = \frac{1}{2}\left(-\widetilde{\beta} + \sqrt{\widetilde{\beta}^2 + 4\widetilde{E}}\right)$, we get 4-eigenstates (first kind of Bessel function).

$$\begin{aligned} (I) & \begin{pmatrix} J_m\left(\gamma_1\widetilde{\rho}_r\right)e^{im\varphi} \\ -iJ_{m-1}\left(\gamma_1\widetilde{\rho}_r\right)e^{i(m-1)\varphi} \end{pmatrix}, (II) \begin{pmatrix} J_m\left(-\gamma_1\widetilde{\rho}_r\right)e^{im\varphi} \\ iJ_{m-1}\left(-\gamma_1\widetilde{\rho}_r\right)e^{i(m-1)\varphi} \end{pmatrix}, \\ (III) & \begin{pmatrix} J_m\left(\gamma_2\widetilde{\rho}_r\right)e^{im\varphi} \\ iJ_{m-1}\left(\gamma_2\widetilde{\rho}_r\right)e^{i(m-1)\varphi} \end{pmatrix}, (IV) \begin{pmatrix} J_m\left(-\gamma_2\widetilde{\rho}_r\right)e^{im\varphi} \\ -iJ_{m-1}\left(-\gamma_2\widetilde{\rho}_r\right)e^{i(m-1)\varphi} \end{pmatrix} \end{aligned} \tag{A.13}$$

But (I) (II) and (III) (IV) have the same form, therefore we have just 2 independent bases. Besides, the index of m should be integers (including positive and negative), then we have to introduce the second kind of Bessel function "Neumann" to be eigenstates.

$$
(I) \begin{pmatrix} N_m \left(\gamma_1 \widetilde{\rho}_r\right) e^{im\varphi} \\ -iN_{m-1} \left(\gamma_1 \widetilde{\rho}_r\right) e^{i(m-1)\varphi} \end{pmatrix}, (II) \begin{pmatrix} N_m \left(-\gamma_1 \widetilde{\rho}_r\right) e^{im\varphi} \\ iN_{m-1} \left(-\gamma_1 \widetilde{\rho}_r\right) e^{i(m-1)\varphi} \end{pmatrix},
$$
$$
(III) \begin{pmatrix} N_m \left(\gamma_2 \widetilde{\rho}_r\right) e^{im\varphi} \\ iN_{m-1} \left(\gamma_2 \widetilde{\rho}_r\right) e^{i(m-1)\varphi} \end{pmatrix}, (IV) \begin{pmatrix} N_m \left(-\gamma_2 \widetilde{\rho}_r\right) e^{im\varphi} \\ -iN_{m-1} \left(-\gamma_2 \widetilde{\rho}_r\right) e^{i(m-1)\varphi} \end{pmatrix}
\tag{A.14}
$$

In order to get more clearly physical meaning, we change Bessel functions to Henkel functions: $H_\alpha^{(1)}(x) = J_\alpha(x) + iN_\alpha(x)$ and $H_\alpha^{(2)}(x) = J_\alpha(x) - iN_\alpha(x)$.

Finally, we get total eigenfunction

$$
\Psi = a \begin{pmatrix} H_m^{(1)} \left(\gamma_1 \widetilde{\rho}_r\right) e^{im\varphi} \\ -iH_{m-1}^{(1)} \left(\gamma_1 \widetilde{\rho}_r\right) e^{i(m-1)\varphi} \end{pmatrix} + b \begin{pmatrix} H_m^{(2)} \left(\gamma_1 \widetilde{\rho}_r\right) e^{im\varphi} \\ -iH_{m-1}^{(2)} \left(\gamma_1 \widetilde{\rho}_r\right) e^{i(m-1)\varphi} \end{pmatrix}
$$
$$
+c \begin{pmatrix} H_m^{(1)} \left(\gamma_2 \widetilde{\rho}_r\right) e^{im\varphi} \\ iH_{m-1}^{(1)} \left(\gamma_2 \widetilde{\rho}_r\right) e^{i(m-1)\varphi} \end{pmatrix} + d \begin{pmatrix} H_m^{(2)} \left(\gamma_2 \widetilde{\rho}_r\right) e^{im\varphi} \\ iH_{m-1}^{(2)} \left(\gamma_2 \widetilde{\rho}_r\right) e^{i(m-1)\varphi} \end{pmatrix}
\tag{A.15}
$$

Appendix B

Solve the finite width mesoscopic ring Hamiltonian with DSO coupling after considering magnetic flux

In order to consider adding the magnetic flux in our system, we should correct the momentum: (a) $p \rightarrow p - eA$; (b) $k \rightarrow k - \frac{eA}{\hbar}$, where A is the vector potential chosen as the axial gauge. And the corresponding magnetic flux is $\frac{\Phi}{\Phi_0} = \frac{2\pi e A_\varphi \rho}{h} = \frac{e A_\varphi \rho}{\hbar}$ in units of flux quantum $\Phi_0 = \frac{h}{e}$. (The magnetic flux $\Phi = \int \overrightarrow{B} \cdot \overrightarrow{n} \, da = \int \left(\overrightarrow{\nabla} \times \overrightarrow{A} \right) da = \oint_c \overrightarrow{A} \cdot d\overrightarrow{l} = \oint_c A_\varphi \rho \, d\varphi = 2\pi A_\varphi \rho$)

Three main expression about the corrections are:

$$
\begin{aligned}
(a) \, (p - eA)^2 &= p^2 - e \left(\widehat{p}\widehat{A} + \widehat{A}\widehat{p} \right) + e^2 A_\varphi^2 = p^2 - 2e A_\varphi p_\varphi + e^2 A_\varphi^2 \\
&= \hbar^2 \left(k^2 - \frac{2e A_\varphi k_\varphi}{\hbar} + \frac{e^2 A_\varphi^2}{\hbar^2} \right) = \hbar^2 \left[k^2 - 2 \left(\frac{\Phi}{\rho \Phi_0} \right) k_\varphi + \left(\frac{\Phi}{\rho \Phi_0} \right)^2 \right]
\end{aligned}
\tag{B.1}
$$

$$
\begin{aligned}
(b) \, k_+ &= \left(k_x - \frac{e A_x}{\hbar} \right) + i \left(k_y - \frac{e A_y}{\hbar} \right) = (k_x + i k_y) - \frac{e}{\hbar}(A_x + i A_y) \\
&= -i e^{i\varphi} \left(\frac{\partial}{\partial \rho} + \frac{i}{\rho} \frac{\partial}{\partial \varphi} + \frac{e A_\varphi}{\hbar} \right) = -i e^{i\varphi} \left(\frac{\partial}{\partial \rho} + \frac{i}{\rho} \frac{\partial}{\partial \varphi} + \frac{\Phi}{\rho \Phi_0} \right)
\end{aligned}
\tag{B.2}
$$

$$
\begin{aligned}
(c) \, k_- &= \left(k_x - \frac{e A_x}{\hbar} \right) - i \left(k_y - \frac{e A_y}{\hbar} \right) = (k_x - i k_y) - \frac{e}{\hbar}(A_x - i A_y) \\
&= -i e^{-i\varphi} \left(\frac{\partial}{\partial \rho} - \frac{i}{\rho} \frac{\partial}{\partial \varphi} - \frac{e A_\varphi}{\hbar} \right) = -i e^{-i\varphi} \left(\frac{\partial}{\partial \rho} - \frac{i}{\rho} \frac{\partial}{\partial \varphi} - \frac{\Phi}{\rho \Phi_0} \right)
\end{aligned}
\tag{B.3}
$$

APPENDIX B. SOLVE THE FINITE WIDTH MESOSCOPIC RING HAMILTONIAN WITH DSO COUPLING AFTER CONSIDERING MAGNETIC FLUX

Note: $\widehat{p}\widehat{A} = -i\hbar\overrightarrow{\nabla}\left(-\frac{A_0}{\rho}\widehat{\varphi}\right) + \widehat{A}\widehat{p} = A_\varphi p_\varphi$

In the following, just like in chapter 2, we guess the form of the total eigenfunction:

$$\Psi = \begin{pmatrix} f_1(\rho)e^{im\varphi} \\ f_2(\rho)e^{i(m-1)\varphi,} \end{pmatrix}. \tag{B.4}$$

where $f_1(\rho)$, $f_2(\rho)$ have to be solved explicitly.

Considering Eq. (B.1), Eq. (B.2), Eq. (B.3) and rewriting the Hamiltonian in polar coordinates with a hard-wall confinement potential:

$$V(\overrightarrow{\rho}, z) = \begin{cases} 0 & \text{for } r_1 < \rho < r_2 \text{ and } |z| < \frac{d}{2} \\ \infty & \text{otherwise} \end{cases} \tag{B.5}$$

the Schrodinger equation $H\Psi = E\Psi$ becomes Eq. (B.6)

$$\begin{cases} \frac{\hbar^2}{2m^*}\left[k^2 - 2\left(\frac{\Phi}{\rho\Phi_0}\right)k_\varphi + \left(\frac{\Phi}{\rho\Phi_0}\right)^2\right]f_1(\rho)e^{im\varphi} + i\beta\left(\frac{\pi}{d}\right)^2 e^{i\varphi}\left(\frac{\partial}{\partial\rho} + \frac{i}{\rho}\frac{\partial}{\partial\varphi} + \frac{\Phi}{\rho\Phi_0}\right)f_2(\rho)e^{i(m-1)\varphi} \\ = Ef_1(\rho)e^{im\varphi} \\ \frac{\hbar^2}{2m^*}\left[k^2 - 2\left(\frac{\Phi}{\rho\Phi_0}\right)k_\varphi + \left(\frac{\Phi}{\rho\Phi_0}\right)^2\right]f_2(\rho)e^{i(m-1)\varphi} + i\beta\left(\frac{\pi}{d}\right)^2 e^{-i\varphi}\left(\frac{\partial}{\partial\rho} - \frac{i}{\rho}\frac{\partial}{\partial\varphi} - \frac{\Phi}{\rho\Phi_0}\right)f_1(\rho)e^{im\varphi} \\ = Ef_2(\rho)e^{i(m-1)\varphi} \end{cases} \tag{B.6}$$

In order to get more clearly formula and prepare for the Numerical analysis, we set some parameters to dimensionless the Hamiltonian: (a) Fermi wave length l_f, (b) Fermi wave vector $k_f = \frac{1}{l_f}$, (c) Fermi energy $E_f = \frac{\hbar^2 k_f^2}{2m^*}$, (d)Del operator in polar coordinates $\nabla = k_f\widetilde{\nabla}$, (e) $p_{\rho,\varphi}^{\pm} = k_f\widetilde{p}_{\rho,\varphi}^{\pm}$, (f) $\widetilde{E} = \frac{E}{E_f}$, (g) $\widetilde{\beta} = \frac{\beta\left(\frac{\pi}{d}\right)^2 \cdot k_f}{E_f}$, (h) $\widetilde{\rho}_r = \frac{\rho}{r_1}$.

APPENDIX B. SOLVE THE FINITE WIDTH MESOSCOPIC RING HAMILTONIAN WITH DSO COUPLING AFTER CONSIDERING MAGNETIC FLUX

$$
\begin{cases}
\left\{ \frac{1}{\widetilde{\rho}} \frac{\partial}{\partial \widetilde{\rho}} \left(\widetilde{\rho} \frac{\partial}{\partial \widetilde{\rho}} \right) - \frac{1}{\widetilde{\rho}^2} \left(m - \frac{\Phi}{\Phi_0} \right)^2 \right\} f_1(\widetilde{\rho}_r) e^{im\varphi} - i\widetilde{\beta} \left(\frac{\partial}{\partial \widetilde{\rho}} - \frac{1}{\widetilde{\rho}}(m - \frac{\Phi}{\Phi_0} - 1) \right) f_2(\widetilde{\rho}_r) e^{im\varphi} \\
\quad = -\widetilde{E} f_1(\widetilde{\rho}_r) e^{im\varphi} \\
\left\{ \frac{1}{\widetilde{\rho}} \frac{\partial}{\partial \widetilde{\rho}} \left(\widetilde{\rho} \frac{\partial}{\partial \widetilde{\rho}} \right) - \frac{1}{\widetilde{\rho}^2} \left(m - 1 - \frac{\Phi}{\Phi_0} \right)^2 \right\} f_2(\widetilde{\rho}_r) e^{i(m-1)\varphi} - i\widetilde{\beta} \left(\frac{\partial}{\partial \widetilde{\rho}} + \frac{1}{\widetilde{\rho}} \left(m - \frac{\Phi}{\Phi_0} \right) \right) f_1(\widetilde{\rho}_r) e^{i(m-1)\varphi} \\
\quad = -\widetilde{E} f_2(\widetilde{\rho}_r) e^{i(m-1)\varphi}
\end{cases}
\tag{B.7}
$$

Let $q = m - \frac{\Phi}{\Phi_0}$, Eq. (B.7) become

$$
\begin{cases}
\left\{ \frac{1}{\widetilde{\rho}} \frac{\partial}{\partial \widetilde{\rho}} \left(\widetilde{\rho} \frac{\partial}{\partial \widetilde{\rho}} \right) - \frac{q^2}{\widetilde{\rho}^2} \right\} f_1(\widetilde{\rho}_r) e^{im\varphi} - i\widetilde{\beta} \left(\frac{\partial}{\partial \widetilde{\rho}} - \frac{1}{\widetilde{\rho}}(q-1) \right) f_2(\widetilde{\rho}_r) e^{im\varphi} = -\widetilde{E} f_1(\widetilde{\rho}_r) e^{im\varphi} \\
\left\{ \frac{1}{\widetilde{\rho}} \frac{\partial}{\partial \widetilde{\rho}} \left(\widetilde{\rho} \frac{\partial}{\partial \widetilde{\rho}} \right) - \frac{(q-1)^2}{\widetilde{\rho}^2} \right\} f_2(\widetilde{\rho}_r) e^{i(m-1)\varphi} - i\widetilde{\beta} \left(\frac{\partial}{\partial \widetilde{\rho}} + \frac{q}{\widetilde{\rho}} \right) f_1(\widetilde{\rho}_r) e^{i(m-1)\varphi} = -\widetilde{E} f_2(\widetilde{\rho}_r) e^{i(m-1)\varphi}
\end{cases}
\tag{B.8}
$$

Since these differential equations have the forms of Bessel equation and the recurrence relation, we can choose the Bessel functions as the spinor part eigenfunctions. Therefore,

$$
\begin{cases}
-\gamma^2 A J_q(\gamma\widetilde{\rho}_r) - i\widetilde{\beta} \left[-\gamma B J_q(\gamma\widetilde{\rho}_r) \right] = -\widetilde{E} A J_q(\gamma\widetilde{\rho}_r) \\
-\gamma^2 B J_{q-1}(\gamma\widetilde{\rho}_r) - i\widetilde{\beta} \left[\gamma A J_{q-1}(\gamma\widetilde{\rho}_r) \right] = -\widetilde{E} B J_{q-1}(\gamma\widetilde{\rho}_r)
\end{cases}
\tag{B.9}
$$

where A and B are the coefficients of the two eigenfunction components.

Comparing with above couple equations, we find that the ratio of the coefficients $R = \frac{B}{A} = \pm i$, then we get two branches of wave functions

$$
\Psi = \begin{bmatrix} J_q(\gamma\widetilde{\rho}_r) e^{im\varphi} \\ i J_{q-1}(\gamma\widetilde{\rho}_r) e^{i(m-1)\varphi} \end{bmatrix}, \Psi = \begin{bmatrix} J_q(\gamma\widetilde{\rho}_r) e^{im\varphi} \\ -i J_{q-1}(\gamma\widetilde{\rho}_r) e^{i(m-1)\varphi} \end{bmatrix}.
\tag{B.10}
$$

Appendix C

Prove state $|\psi_a\rangle$ and $|\psi_b\rangle$ do not mixing

Assuming $m' > 0$, then we can define $|\psi_a\rangle$ and $|\psi_b\rangle$:

$$|\psi_a\rangle = c_1 |E_{n,m',\uparrow}\rangle + c_2 |E_{n,m'-1,\downarrow}\rangle \tag{C.1}$$

$$|\psi_b\rangle = c_3 \left|E_{n,-(m'-1),\uparrow}\right\rangle + c_4 |E_{n,-m',\downarrow}\rangle. \tag{C.2}$$

After considering external magnetic flux, the effective correctional Hamiltonian can be defined:

$$H_\Phi = \left(\frac{1}{\rho}\frac{\Phi}{\Phi_0}\right) \begin{pmatrix} \frac{2i}{\rho}\frac{\partial}{\partial\varphi} + \frac{1}{\rho}\frac{\Phi}{\Phi_0} & i\beta e^{i\varphi} \\ -i\beta e^{-i\varphi} & \frac{2i}{\rho}\frac{\partial}{\partial\varphi} + \frac{1}{\rho}\frac{\Phi}{\Phi_0} \end{pmatrix} \tag{C.3}$$

If we integrate the sandwich-matrix, we get the angular-part result is zero:

$$\langle\psi_a| H_\Phi |\psi_b\rangle = \int \left(\frac{1}{\rho}\frac{\Phi}{\Phi_0}\right) F(\rho,\varphi)dv = 0, \tag{C.4}$$

where

$$F\left(\rho,\varphi\right)$$

$$= \begin{pmatrix} f^*_{n,m'}e^{-im'\varphi} & g^*_{n,m'-1}e^{-i(m'-1)\varphi} \end{pmatrix} \begin{pmatrix} \frac{2i}{\rho}\frac{\partial}{\partial\varphi} + \frac{1}{\rho}\frac{\Phi}{\Phi_0} & i\beta e^{i\varphi} \\ -i\beta e^{-i\varphi} & \frac{2i}{\rho}\frac{\partial}{\partial\varphi} + \frac{1}{\rho}\frac{\Phi}{\Phi_0} \end{pmatrix} \begin{pmatrix} f_{n,-(m'-1)}e^{-i(m'-1)\varphi} \\ g_{n,-m'}e^{-im'\varphi} \end{pmatrix}$$

$$= \begin{pmatrix} f^*_{n,m'}e^{-im'\varphi} & g^*_{n,m'-1}e^{-i(m'-1)\varphi} \end{pmatrix} \begin{pmatrix} \left[\left(\frac{2(m'-1)}{\rho} + \frac{1}{\rho}\frac{\Phi}{\Phi_0}\right)f_{n,-(m'-1)} + i\beta g_{n,-m'}\right]e^{-i(m'-1)\varphi} \\ \left[\left(\frac{2m'}{\rho} + \frac{1}{\rho}\frac{\Phi}{\Phi_0}\right)g_{n,-m'} - i\beta f_{n,-(m'-1)}\right]e^{-im'\varphi} \end{pmatrix}$$

$$= \left\{ \begin{array}{l} \left[\left(\frac{2(m'-1)}{\rho} + \frac{1}{\rho}\frac{\Phi}{\Phi_0}\right)f^*_{n,m'}f_{n,-(m'-1)} + i\beta f^*_{n,m'}g_{n,-m'}\right] \\ + \left[\left(\frac{2m'}{\rho} + \frac{1}{\rho}\frac{\Phi}{\Phi_0}\right)g^*_{n,m'-1}g_{n,-m'} - i\beta g^*_{n,m'-1}f_{n,-(m'-1)}\right] \end{array} \right\} e^{-i(2m'-1)\varphi}.$$

Appendix D

Demonstrate that the energy level split into the higher energy part and the lower energy part

If $\frac{\Phi}{\Phi_0}$ is small, H_Φ can be redefine as $H_\Phi^{(1)} = \left(\frac{1}{\rho} \frac{\Phi}{\Phi_0} \right) \begin{pmatrix} \frac{2i}{\rho} \frac{\partial}{\partial\varphi} & i\beta e^{i\varphi} \\ -i\beta e^{-i\varphi} & \frac{2i}{\rho} \frac{\partial}{\partial\varphi} \end{pmatrix}$. The expected

value of $H_\Phi^{(1)}$ with state $|\psi_a\rangle$ is $\langle\psi_a| H_\Phi^{(1)} |\psi_a\rangle = \int F_m(\rho,\varphi)dv$,

$$F_m(\rho,\varphi)$$

$$= \begin{pmatrix} f_{n,m}^*(\rho)e^{-im\varphi} & g_{n,m-1}^*(\rho)e^{-i(m-1)\varphi} \end{pmatrix} \left(\frac{1}{\rho}\frac{\Phi}{\Phi_0} \right) \begin{pmatrix} \frac{2i}{\rho}\frac{\partial}{\partial\varphi} & i\beta e^{i\varphi} \\ -i\beta e^{-i\varphi} & \frac{2i}{\rho}\frac{\partial}{\partial\varphi} \end{pmatrix} \begin{pmatrix} f_{n,m}(\rho)e^{im\varphi} \\ g_{n,m-1}(\rho)e^{i(m-1)\varphi} \end{pmatrix}$$

$$= \left(\frac{1}{\rho}\frac{\Phi}{\Phi_0} \right) \begin{pmatrix} f_{n,m}^*(\rho)e^{-im\varphi} & g_{n,m-1}^*(\rho)e^{-i(m-1)\varphi} \end{pmatrix} \begin{pmatrix} \left[\frac{-2m}{\rho}f_{n,m}(\rho) + i\beta g_{n,m-1}(\rho) \right]e^{im\varphi} \\ \left[\frac{-2(m-1)}{\rho}g_{n,m-1}(\rho) - i\beta f_{n,m}(\rho) \right]e^{i(m-1)\varphi} \end{pmatrix}$$

$$= \left(\frac{1}{\rho}\frac{\Phi}{\Phi_0} \right) \left\{ \begin{array}{l} -\frac{2}{\rho}\left[mf_{n,m}^*(\rho)f_{n,m}(\rho) + (m-1)g_{n,m-1}^*(\rho)g_{n,m-1}(\rho) \right] \\ +i\beta\left[f_{n,m}^*(\rho)g_{n,m-1}(\rho) - g_{n,m-1}^*(\rho)f_{n,m}(\rho) \right] \end{array} \right\}$$

$$= -\frac{1}{\rho^2}\left(\frac{\Phi}{\Phi_0} \right)\left[(2m-1)N_m + S_z \right] - \left(\frac{1}{\rho}\frac{\Phi}{\Phi_0} \right)\beta S_{y(\varphi=0)}$$

Where

APPENDIX D. DEMONSTRATE THAT THE ENERGY LEVEL SPLIT INTO THE HIGHER ENERGY PART AND THE LOWER ENERGY PART

$$N_m = f_{n,m}^* (\rho) f_{n,m} (\rho) + g_{n,m-1}^* (\rho) g_{n,m-1} (\rho) \tag{D.1}$$

$$S_z = f_{n,m}^* (\rho) f_{n,m} (\rho) - g_{n,m-1}^* (\rho) g_{n,m-1} (\rho) \tag{D.2}$$

$$S_y = i \left[-f_{n,m}^* (\rho) g_{n,m-1} (\rho) e^{-i\varphi} + g_{n,m-1}^* (\rho) f_{n,m} (\rho) e^{i\varphi} \right] \tag{D.3}$$

$$\langle \psi_a | H_\Phi^{(1)} | \psi_a \rangle = \int F_m (\rho, \varphi) dv = - \left(\frac{\Phi}{\Phi_0} \right) \int \left\{ \frac{1}{\rho^2} [(2m - 1) N_m + S_z] + \left(\frac{1}{\rho} \right) \beta S_{y(\varphi=0)} \right\} dv \tag{D.4}$$

If we use $|\psi_b\rangle$ instead of $|\psi_a\rangle$ repeating the same process, we will get the same result:

$$\langle \psi_a | H_\Phi^{(1)} | \psi_a \rangle = \langle \psi_b | H_\Phi^{(1)} | \psi_b \rangle = - \left(\frac{\Phi}{\Phi_0} \right) \int \left\{ \frac{1}{\rho^2} [(2m - 1) N_m + S_z] + \left(\frac{1}{\rho} \right) \beta S_{y(\varphi=0)} \right\} dv \tag{D.5}$$

Appendix E

The table of the eigenstates

Bibliography

[1] E. I. Rashba, Sov. Phys. Solid State 2, 1109 (1960); Y. A. Bychkov and E. I. Rashba,J. Phys. C 17, 6039 (1984).

[2] G. Dresselhaus, Phys. Rev. 100, 580 (1955).

[3] Fabrizio M. Alves, C. Trallero-Giner, V. Lopez-Richard, and G. E. Marques, Phys. Rev. B 77, 035434 (2008)

[4] Supriyo Datta and Biswajit Das, Appl. Phys. Lett. 56, 665 (1990).

[5] Topics in advanced quantum mechanics, Barry R. Holstein (Addison Wesley).

[6] Spin-Orbit Coupling in Two-Dimensional Electron and Hole systems, edited by Roland Winkler (Springer-Verlag,Berlin, 2003).

[7] M. Buttiker, Y. Imry, and R. Landauer, Phys. Lett. 96A, 365 (1983)

[8] Introduction to solid state physics, edited by Charles kittel (Wiley).

[9] R. Landauer and M. Buttiker, Phys. Rev. Lett. 54, 2049 (1985)

[10] J. Splettstoesser, M. Governal, and U. Zulicke, Phys. Rev. B 68, 165341 (2003)

[11] F. Schutz, M. Kollar, and P. Kopietz, Phys. Rev. Lett. 91, 017205 (2003)

[12] J. M. Garcia, G. Medeiros-Ribeiro, K. Schmidt, T. Ngo, J. L. Feng, A. Lorke, J. Kotthaus, and P. M. Petroff, Appl. Phys. Lett. 71, 2014 (1997).

[13] A. Lorke and R. J. Luyken, Physica B 256-258, 424 (1998); A. Lorke, R. J. Luyken, M. Fricke, J. P. Kotthaus, G. Medeiros-Ribeiro, J. M. Garcia, and P. M. Petroff, Microelectron. Eng. 47, 95 (1999).

[14] H. Pettersson, R. J. Warburton, A. Lorke, K. Karrai, J. P. Kotthaus, J. M. Garcia, and P. M. Petroff, Physica E (Amsterdam) 6, 510 (2000).

[15] A. Lorke, R. J. Luyken, A. O. Govorov, J. P. Kotthaus, J. M. Garcia, and P. M. Petroff, Phys. Rev. Lett. 84, 2223 (2000).

[16] R. J. Warburton, C. Schaflein, D. Haft, F. Bickel, A. Lorke, K. Karrai, J. M. Garcia, W. Schoenfeld, and P. M. Petroff, Nature(London) 405, 926 (2000).

[17] J. C. Ahn, K. S. Kwak, B. H. Park, H. Y. Kang, J. Y. Kim, and O. D. Kwon, Phys. Rev. Lett. 82, 536 (1999).

[18] A. Lorke and R. J. Luyken, Physica B 256, 424 (1998).

[19] L. Villegas-Lelovsky, C. Trallero-Giner, M. Rebello Sousa Dias, V. Lopez-Richard, and G. E. Marques, Phys. Rev. B 79, 155306 (2009).